

DR. ROLF SCHÜTZ (Orcid ID : 0000-0003-2410-6128)

Article type : Original Article

Bio-derived hydroxystearic acid ameliorates skin age spots and conspicuous pores

Rolf Schütz¹, Anthony V. Rawlings², Eliane Wandeler¹, Eileen Jackson¹, Solène Trevisan³, Jean-Marc Monneuse⁴, Igor Bendik¹, Marco Massironi⁵, Dominik Imfeld¹

¹DSM Nutritional Products Ltd., CH-4143 Kaiseraugst, Switzerland. ²AVR Consulting Ltd., Northwich, UK. ³Newtone Technologies, Lyon, France, ⁴Phylogene SA, Bernis, France, ⁵Cutech Srl, Padova, Italy.

Corresponding author: rolf.schuetz@dsm.com, Phone +41 61 815 8266, Fax +41 61 815 8740

Anthony V. Rawlings tonyrawlings@avrconsultingltd.com

Eliane Wandeler eliane.wandeler@dsm.com

Eileen Jackson eileen.jackson@dsm.com

Solène Trevisan strevisan@newtone.fr

Jean-Marc Monneuse jm.monneuse@phylogene.com

Igor Bendik igor.bendik@dsm.com

Marco Massironi marco.massironi@cutech.it

Dominik Imfeld Dominik.Imfeld@dsm.com

KEYWORDS: Skin physiology/structure, computer modelling, chemical synthesis, age spots, pores, hydroxystearic acid.

Introduction

As we age, our skin develops visible signs of aging [1]. In contrast to other body organs, the skin as our first line of defense is constantly exposed to challenges from the environment. Ultraviolet (UV) irradiation, and to some extent visible light, climate changes and pollution are the major external environmental contributory factors whereas psychological stress, fatigue and dietary habits are internal stress factors also contribute to the skin aging exposome [2]. Recent global consumer surveys on the primary cosmetic concerns of women have identified that not only are the presence of

This article has been accepted for publication and undergone full peer review but has not been through the copyediting, typesetting, pagination and proofreading process, which may lead to differences between this version and the Version of Record. Please cite this article as doi: 10.1111/ics.12529

This article is protected by copyright. All rights reserved.

wrinkles and uneven skin tone perceived as major signs of aging but also the presence of conspicuous skin pores (unpublished data). Moreover, there are ethnic differences in frequency of expression of such skin problems, with the presence of enlarged pores and age spots being of major cosmetic concern for Asian women [3-5].

Visible skin pores are enlarged funnel-shaped or cylindrical openings of the pilosebaceous follicles that become more dilated and more conspicuous caused by the continuous hydrostatic pressure induced by sebum on the pilosebaceous duct in the presence of decreased skin elasticity or slackening in the surrounding areas of the duct caused by aging [6]. Morphological changes in the dermoepidermal junction (DEJ) are also clearly observed in subjects with conspicuous pores *in vivo* [5]. Moreover, abnormal keratinocyte differentiation has also been reported with the accumulation of parakeratotic nucleated corneocytes clearly indicative of UV light irradiation damage to the epidermal keratinocytes [7].

Age spots are benign flat spots of dark pigmentation on the skin occurring especially among older people [8-10]. Prolonged and chronic exposure to UV light and pollutants can accelerate the production of melanin by hyperactive melanocytes [11-13]. However, evidence indicates that the bulk of melanin is inherited only by the non-differentiating daughter cell post mitosis in progenitor keratinocytes via asymmetric organelle inheritance. Moreover, this preferred pattern of melanin distribution can switch to a symmetric or equal daughter cell inheritance mode under conditions of stress [14].

Secretion of melanogenic paracrine factors can also be derived from both keratinocytes and fibroblasts as a result of UV-induced oxidative stress [15, 16]. Downregulation of genes involved in epidermal differentiation have also been reported in age spots as well as decreased expression of filaggrin and involucrin [17]. Increased expression of the basal type keratins 5 & 10 also indicates poor keratinocyte differentiation in age spots [18]. Increased p53 levels also contribute to defective epidermal differentiation [19]. The most recent hypothesis is that the increased proliferation of basal keratinocytes combined with decreased turnover of suprabasal keratinocytes puts a backwards pressure on the DEJ leading to an exaggerated formation of rete ridges, similar to that in age spots, which also leads to reduced melanin processing upwards from the basal layer of the epidermis [18]. The poor turnover of the suprabasal cells is also suggested by increased numbers of cell layers in the stratum corneum (SC) in age spots.

Here, we report on a sustainable source and synthesis of chiral (R)-10-hydroxystearic acid (HSA) that reduces the appearance of both age spots and conspicuous pores *in vivo*. From *in vitro* and *ex vivo* studies we also show that non-UV absorbing HSA mitigates the negative effects of UV stress on skin by reducing p53 activation and MMP-1 levels. In addition, it increases collagen type I & III synthesis. Proteomic analysis of proteins secreted from fibroblasts corroborates mechanisms that reduce melanogenesis, increase fibroblast activity and stimulate keratinocyte differentiation. These proteins

will counter abnormal keratinization, increased melanogenesis and pilosebaceous pore wall slackening associated with age spots and conspicuous pores. HSA is also identified through *in silico* approaches and reporter gene assays to be a PPAR α agonist.

Materials and Methods

Synthesis of 10-hydroxystearic acid (HSA)

In brief, 10% vegetable oleic acid (81%, KLK OLEO, Emmerich, Germany) and 10% cell-free extract containing regio- and enantioselective oleate hydratase (EC 4.2.1.53, DSM Chemical Technology, Geleen, Netherlands) were added to phosphate buffer (1.6 L, 100 mM, pH = 6.5) in a bioreactor and stirred at constant pH and 37°C until $\geq 95\%$ conversion was reached (approx. 24 h). Ethyl acetate was added to the mixture and heated to 60°C while gently stirring followed by crystallization. Filtration and drying of the obtained, white solid material resulted in the enantiopure (*R*)-10-hydroxyoctadecanoic acid (HSA) in 81% yield and 99.8% purity (% w/w, GC-FID, HP-5MS MS, Agilent, Basel, Switzerland). The enantiomeric excess was found to be $>99\%$ determined by chiral HPLC analysis (Chiracel OD-H, Daicel, Illkirch, France) after derivatization as methyl ester. The melting point of the resulting white powder was 86.5 °C. Commercial material (DSM Nutritional Products Ltd, Switzerland) is available with the INCI name hydroxystearic acid.

Experimental Strategy

To determine the effect of HSA on age spot and conspicuous pore reduction we examined extracellular matrix marker production (Collagen type I & III) together with degradative enzymes (MMP-1), reduction of markers of UV damage (sunburn cells and p53), the secretome of fibroblast markers that may influence both keratinocytes and melanocytes and clinically. Moreover, the likely mechanistic target of action was identified as PPAR α from *in silico* and transactivation assays.

Measurement of total cellular Collagen type I and III contents in normal human fibroblasts

Human dermal fibroblasts obtained from adult skin were seeded into 96-well plates (4000 cells/well) and cultured in Dulbecco's Modified Eagle's Medium high glucose (DMEM, Gibco Invitrogen, Basel, Switzerland) containing 10% fetal calf serum (FCS; Amimed BioConcept, Allschwil, Switzerland) and 1% penicillin/streptomycin (P/S; Invitrogen, Switzerland) at 37°C with 5% CO₂ for 24 h. Subsequently the cells were starved in DMEM low-glucose containing 0.2% FCS and 1% P/S for 2.5 days. Starvation medium was then refreshed together with the addition of the solubilized test compounds and incubated for another 48 h. Thereafter, HSA was diluted in the culture medium from a 10 mM dimethylsulphoxide (DMSO) stock solution. Transforming growth factor beta 1 (TGF- β 1; PeproTech, Hamburg, Germany) was used as positive control. After compound incubation cells were fixed in Dulbecco's Phosphate-Buffered Saline (DPBS, Gibco Invitrogen, Switzerland) containing 4% formaldehyde (Life Technologies, Zug, Switzerland) for 15 min and permeabilized with 0.1% Triton-X100 (Sigma Aldrich, Buchs, Switzerland) in DPBS for 90 sec. Collagen type I or III were detected

using mouse anti human collagen I antibody (Millipore, Switzerland) and rabbit anti-human type III collagen (BioTrend, Cologne, Germany), respectively, followed by a AlexaFluor 488-conjugated secondary antibody (goat anti-mouse or anti-rabbit IgG, Life Technologies, Zug, Switzerland). We counterstained the nuclei with 4',6-diamidino-2-phenylindole (DAPI, Sigma-Aldrich, Buchs, Switzerland). Image acquisition and quantitative analysis was performed using an ArrayScan® VTI HCS imaging system (Thermo Scientific, Waltham, MA, USA) with 49 pictures per well with 10X objective. Collagen was measured intracellularly, and the fluorescence intensity values were normalized to the cell count. Data are based on a minimum of three independent measurements and were represented as mean values \pm SEM (Student-t test, significance $p < 0.01$ vs medium control).

Ex vivo Skin Sampling and Treatment

Human skin from abdominal plastic surgery was obtained from healthy Caucasian donors after their informed consent and was used for the analysis of collagen type III, sunburn cells, MMP-1 and p53. Skin samples of 8x3 mm (diameter x thickness) were maintained in an air-liquid interface in contact with culture medium (modified Williams' E medium, Thermo Fisher Scientific, Waltham, MA, USA) up to 6 days. Six skin samples for each treatment were cultured to perform the collagen, sunburn cell, and p53 analyses and two samples for the skin viability and MMP-1 expression. For MMP-1, sunburn cells, and p53 analysis the test samples (4 μ l, 0.33 and 3.30 mM) were topically applied in DMSO as vehicle on the skin biopsies (8 mm diameter) 1 and 24 h prior to UVB irradiation (1 J cm^{-2}) and covered with 7 mm diameter delivery membrane (CoTran, 3M, Italy). The sensor-controlled BIO-SUN irradiation system (Vilber Lourmat, Eberhardzell, Germany) equipped with two T-30.M tubes (30 W, intensity 3 mW cm^{-2}) was used to irradiate the skin with UVB light. The UV emission spectrum ranged from 280 to 400 nm of which 62% emission was in the UVB range (280–320nm, peak maximum 312 nm) and elongated in the UVA range (320–400 nm).

Ex vivo Skin Analyses

Skin viability: After 6 days of incubation, two skin punches have been weighted and, if necessary, reduced in the dermal portion, to have approximately the same weight for all samples. Samples were processed with methylthiazolyldiphenyl-tetrazolium bromide (MTT) according to supplier's instructions (Roche Applied Science, Rotkreuz, Switzerland). Skin viability was measured with a plate reader at a wavelength of 570 nm.

Type III Collagen quantification: Two sections (n=12) from six skin samples were immunostained with monoclonal mouse anti-collagen III (Sigma-Aldrich, cat#C7805, Buchs, Switzerland) and the Alkaline Phosphatase/RED Detection System (Dako #K5005; Agilent Technologies, Glostrup, Denmark). The amount of the antigen present in each slide was evaluated by the intensity and the distribution of the red staining within a selected area of the dermis using ImageJ (NIH, Bethesda; MD, USA).

Quantification of MMP1 expression by reverse transcription quantitative polymerase chain reaction (RT-qPCR): Total RNA was extracted from full-thickness skin using RNAeasy mini kit for fibrous tissues (Qiagen, Hilden, Germany) following the manufacturer's instructions. After quantification, 400 ng of total RNA was retro-transcribed using random hexamers and Superscript III (Invitrogen,

Darmstadt, Germany). The cDNA was used to perform a real-time PCR (SybrGreen protocol) with specific primers for the evaluation of MMP1 expression. ubiquitin and YWHAZ (Tyrosine 3-Monooxygenase/Tryptophan 5-Monooxygenase Activation Protein Zeta) were used as reference genes for data normalization. Data acquisition and statistical analysis of RT-qPCR was performed on RotorGene thermal cycler (Corbett Life Science, Mortlake, Australia) and REST 2009 V2.0.13 software (Qiagen, Darmstadt, Germany).

Sunburn cell (SBC) quantification: Haematoxylin-Eosin (H&E) staining was performed on skin sections to count SBC or apoptotic cells per millimeter of epidermis after analyzing twelve different sections per treatment.

p53 protein quantification: Skin sections were stained with the monoclonal mouse anti-p53 antibody (Abcam, #ab7757, USA). The p53-positive cells were counted, and the obtained values were divided upon the area covered by epidermis. Two slides of each skin sample were processed by image acquisition and related analysis (i.e. 12 images for each test treatment).

Statistical analysis of and ex vivo data: All quantitative data were summarized in terms of the mean score and standard error of mean (SEM) for each treatment. Differences between groups were evaluated by One-way ANOVA with permutation test followed by pairwise post-hoc comparisons Dunnett's permutation test and pairwise post hoc comparisons-Tukey's HSD permutation tests.

Mass-spectrometry-based proteomics of fibroblast secretome

Human dermal fibroblasts (HDF) from a biopsy of an adult female donor (Fb-D) were maintained in Dulbecco's modified Eagle's medium high glucose (DMEM), 10% fetal calf serum (FCS) and 1% penicillin/streptomycin (P/S). Cells were cultivated at 37°C, 5% CO₂-air atmosphere. HDF were seeded in 6 well plates (120'000 cells per well) and cultured for 24 hours in DMEM 10% FCS 1% P/S, then starved in DMEM low glucose 0.2% FCS, 1% P/S for 2.5 days. Starvation medium was then replaced, 5 µM HSA was added and incubated for 48 h. The preparation of the extracellular secreted proteins from the conditioned media was performed. using 20 mM ammonium hydroxide and stringent washing with water [20] . Secreted protein isolates obtained from the cell culture conditioned media were dissolved in 600 µl of 50 mM ammonium bicarbonate buffer containing 0.5 µg of trypsin culture plate wells. Plates were incubated 1.5 h at 37°C. Total protein content was determined using the BCA kit from Thermo Scientific (Illkirch, France). Lysates from same sample were pooled and acidified to block trypsin activity. Lysates were evaporated to dryness (SpeedVac, Thermo Scientific). Proteins were then reduced (DTT) and alkylated (IAA) and trypsin added a second time to complete proteins digestion. For all samples, peptides were purified by SPE chromatography (C18), dried and solubilized in 100 µl of 0.1% formic acid aqueous solution. Peptides digests (500 ng per run) were analyzed by Eksigent Ultra Plus nano-LC 2D HPLC coupled to a TripleTOF 5600 (AB Sciex, Framingham, USA) mass spectrometer interfaced to a nano-spray III source, according to method described in *Voegeli et al.* [21]. The absolute signal of peptide or protein was calculated by summing the extracted area of all unique fragment ions as described in *Gillet et al.* [22].

PPAR transactivation assays and EC₅₀ determination

A one-hybrid-system, using hybrid constructs of GAL4 DNA-binding part coupled to PPAR α , PPAR β or PPAR γ ligand binding domains together with a luciferase reporter and a renilla-expressing plasmid, was applied. For transient transfections, white 96-well cell culture plates with clear bottom (Corning, Basel, Switzerland) were used. 7.5×10^4 HEK293 cells per well were plated in minimum essential medium (Eagle) at 37°C in 5% CO₂ without phenol red supplemented with 10% charcoal-treated fetal bovine serum (HyClone Laboratories, Inc., Logan, UT, USA). The cells were transiently transfected at 70-80% confluence by polyethylene-mine-based transfection for 5 hours at 37°C, 5% CO₂, which was followed with respective stimulations of the applied compounds dissolved in DMSO (0.45% final DMSO concentration in the wells). The GW7647 compound was used as a reference for human PPAR α . Stimulations lasted 16 h according to established protocols. Transfection efficiency was adjusted to renilla expression (Promega AG, Dübendorf, Switzerland). All concentrations were tested in three biological replicates. The "dose response for one site" was applied in a curve fitting model according to the formula: $y = A + ((B - A) / (1 + ((10C) / x)^D))$, whereas A is the minimum y-value, B the maximum y-value, C Log EC₅₀ and D the slope factor. The data was fitted by XLfit (<http://www.idbs.com>) using the Levenburg Marquardt algorithm.

Molecular modeling of the interaction of HSA with PPAR α .

The ligand binding domain of PPAR alpha was retrieved from the RSCB database (PDB: 3SP6) and prepared for modelling studies using a protein preparation wizard (Maestro version 11.0.015, Schrödinger, LLC, New York, NY, 2016). In short, bond orders were set, hydrogens were added, disulphide bridge were created, all water molecules were removed, and hydrogen bonds were optimized using the automated procedure. HSA was docked to the ligand binding domain (Glide, LLC, New York, NY, 2016) and the Standard Precision (SP) setting was used. For docking, multiple conformers of HSA were generated (Confgen, LLC, New York, NY, 2016). Among the top ranked different binding poses generated, the best pose was selected based on visual inspection. Figures were prepared using the PyMOL Molecular Graphics System, Version 1.8.0.4 Schrödinger, LLC.

Full-face, double-blind, vehicle-controlled, parallel-group in vivo study for the effects of HSA on conspicuous pores and age spots.

The study was authorized by the new substance release committee (DSM Nutritional Products, Kaiseraugst, Switzerland) and was conducted in accordance with the Declaration of Helsinki Principles. Written informed consent was collected from all volunteers before enrollment. Before the start of the study healthy volunteers were advised not to use any cosmetic treatments for 3 days. Two panels with 42 Caucasian females with Fitzpatrick skin phototypes II-III were recruited to apply 1% (33 mM) HSA in a cosmetic product formulation (Table I) or the vehicle formulation, respectively, on the face twice daily for 8 weeks. Thirty-seven completed the study and were included in the final analysis from the product group (aged 38 to 65, mean 53.4 ± 7.6 yrs) and 38 in the placebo group (aged 34 to 65, mean 54.4 yrs ± 7.2 yrs). No other topical leave-on product was authorized on face during the study and only a specified cleansing milk was allowed (INCI list: AQUA, PARAFFINUM

LIQUIDUM, PROPYLENE GLYCOL, ALCOHOL DENAT., GLYCERYL STEARATE SE, POLYSORBATE 60, SORBITAN STEARATE, CAPRYLYL GLYCOL, CARBOMER).

Table I describes product formulation and corresponding vehicle without HSA that was used in the clinical study.

Subjects were acclimatized for 30 min at a temperature of $24 \pm 2^\circ\text{C}$ and $35 \pm 10\%$ relative humidity before any images were taken. Full face cross and parallel polarized VISIA-CR images (Canfield Scientific, Parsippany, NJ, USA) were assessed at baseline, 4, and 8 weeks during January 19th to March 15th, 2016 in Northern Germany. Image analysis and statistics on conspicuous facial pores and solar lentigines were performed with calibrated VISIA images (Newtone, Lyon, France). Three pigmented spots were selected on the chosen profile of each subject from the cross-polarized images with the largest area and the best contrast. The contrast was calculated from the difference of the ITA° values (individual topological angle based on CIEL*a*b values) of the surrounding skin minus the age spot. For the conspicuous pores analysis, the parallel-polarized images were used to see distinctly the pores and defined areas near the nose on each image for each subject. After segmentation, the identified pores could be analyzed in terms of area, depth, and volume.

Statistical analysis of in vivo data:

For age spots the ΔITA° were expressed as mean values \pm SEM and significance level $p < 0.05$ product vs vehicle was determined by Student t-test. For pores the surface and volume differences of conspicuous pores for product and vehicle treatment were compared to T=0 and expressed in mean \pm SEM by Shapiro-Wilk test followed by a Mann-Whitney test using significance level of $p < 0.05$ Product vs Vehicle.

Results

Synthesis and structural characterization

The hydration of oleic acid was catalyzed by the oleate hydratase (EC:4.2.1.53) from a crude cell-free extract produced in a proprietary process resulting in the enantiopure (*R*)-10-hydroxystearic acid in high yield (81%) and purity (99.8%) after crystallization. Reproducibility was shown by 5 consecutive batches with similar productivity and quality analyzed by GC-MS and ¹H-NMR (data not shown).

HSA stimulated Collagen type I and type III synthesis in human skin fibroblasts

We assessed the stimulatory effect of HSA on collagen type I and type III on primary human dermal fibroblasts after 48 hours of incubation. HSA significantly and dose-dependently induced collagen on human dermal fibroblasts (Fig.1). The amount of newly synthesized collagen type I almost doubled compared to the medium control when HSA was added at 5 μM concentration ($p < 0.01$). In addition, collagen type III synthesis was stimulated up to 244% in HSA (5 μM) treated fibroblasts versus untreated cells ($p < 0.01$).

HSA markedly induced ex vivo synthesis of collagen type III

Human skin biopsies from plastic surgery were utilized to verify the modulatory activities of HSA. The test material in DMSO was applied topically and renewed daily for 6 days. The immunohistochemical (IHC) staining in the prepared skin sections (Fig. 2A) showed that HSA at concentrations between 0.33 mM and 3.3 mM (= 0.1 w/w%) significantly stimulated the formation of collagen type III up to 57% compared to the control at day six (Fig. 2B).

UV-induced MMP-1 expression, sunburn cell formation and p53 protein were reduced ex vivo by HSA

The gene expression of MMP-1 in untreated skin explants was analyzed 24 hours after the UV irradiation (1 J cm^{-2}) and was shown to be upregulated by a factor of 3.4 (Fig.3A) compared to the non-irradiated control. A significant decrease of 83% in MMP-1 expression was observed in ex vivo skin topically treated with 0.33 mM (0.1%) HSA compared the irradiated vehicle control ($p < 0.05$). In another experiment, the sunburn cell (SBC) formation was quantified 24 hours post-UVB (1 J cm^{-2}) by H&E staining. As expected, UVB irradiation significantly increased the incidence of sunburn cells more than two-fold vs. non-irradiated control (Fig. 3B). Interestingly, 0.33 mM (0.1%) HSA reduced the formation of sunburn cells by 49% compared to the vehicle-treated, UVB-irradiated controls. Next, we tested the effect of HSA on UV-induced up-regulation of the stress marker protein p53 when topically applied on human skin biopsies. Indeed, 24 hours after UVB irradiation (1 J cm^{-2}) immunostained skin sections showed an 80-fold induction of p53 compared to the non-irradiated control skin (Fig. 4). HSA inhibited UV-induced p53 formation by 46% vs irradiated vehicle control skin.

Fibroblast secretome modified by HSA

Considering factors that influence melanogenesis and thereby the skin lightening activity of HSA. As shown in Table II, HSA appears to modulate many of the proteins in the Wnt-related Integration site (WNT) signaling pathway that would normally increase melanogenesis. Typical of these is reduced levels of secreted frizzled-related protein 1 (sFRP1; 0.77X) and increased antagonist proteins such as Insulin-like growth factor binding protein 3 (IGFBP2; 15.07X) and Angiopoietin-related protein 4 (ANGPTL4; 2.9X). However, Dickkopf-related protein 1 (DKK1) also a WNT antagonist had slightly lower levels following treatment (0.78X). Protein CYR61 also inhibits melanocyte growth and increased levels (1.45X) were observed with HSA treatment. Gremlin-1 (0.48X) a bone morphogenic binding protein that increases melanogenesis was also decreased as was adrenomedullin (0.36X) a melanocyte dendrite branching factor. Semaphorin3A (Sema3A; 1.35X) was increased whereas the 3B/3D isoforms (0.72X; 0.63X) were decreased and their changes influence nerve growth and melanogenesis. Similarly, IGFBP3, fibroblast growth factor 5 (FGF5) and nectin-1 increased in pigmented disorders in melanoma and their decreases observed with HSA are consistent with a skin lightening effect (0.90X, 0.76X and 0.71X). As transforming growth factor beta ($\text{TGF}\beta$) is normally associated with decreased skin pigmentation then reductions in Latent-transforming growth factor beta-binding protein 2 (LTBP2) (0.66X; Table III) caused by HSA will help

Accepted Article

this. Also increased levels of gremlin-2 (1.74X; Table III) probably inhibit certain BMP isoforms, e.g. BMP6 to reduce melanogenesis [23]. A disintegrin and metalloproteinase with thrombospondin motifs 23 (ADAM 23), MMP3 and serine peptidases are known to be increased in solar lentigo's and we observed many decreases in proteases that may be associated with decreased melanogenesis or increased protease inhibitors (Table IV & V). Alpha-2-antiplasmin (3.90X) is of interest as plasmin destruction of the DEJ is associated with increased melanogenesis. Increased Tissue inhibitor of metalloproteinase 3 (TIMP3; 1.66X) may also control the excessive proteolysis and melanogenesis activation. Moreover, MMP14 (0.65X) controls melanocyte migration and the reduction by HSA can account for decreased age spot expression.

Considering factors that influence keratinocyte differentiation and thereby the strengthening pore wall elasticity activity of HSA. As shown in Table II, changes in the Insulin-like growth factor 1 (IGF-1)/ Insulin-like growth factor binding protein (IGFBP) signaling pathway were observed with lower levels of IGFBP3 (0.90X) following HSA treatment but also dramatic increases in another IGF-1 binding protein IGFBP2 (15.07X) consistent with changes in pores. Moreover, increases in the levels of Midkine (15.74X), the highest secreted protein, ANGPTL4 (2.90X), TGFBI (1.41X) and Sema3A (1.35X) maybe associated with increased keratinocyte differentiation and Isoform delta of stromal cell-derived factor 1 (SDF1A; 3.94X) with keratinocyte proliferation. Adrenomedullin was decreased (0.36X).

Considering factors that influence fibroblasts and ECM production and thereby the strengthening pore wall elasticity activity of HSA. The above reported changes in midkine and TGFBI can improve fibroblast migration and proliferation together with glycosaminoglycan synthesis. Increased levels of connective tissue growth factor (CTGF; 2.29X) will increase procollagen production to help with pore wall structure and reductions in complement C1q tumor necrosis factor-related protein 3 (C1QTNF3; 0.34X) will help as this factor inhibits TGF β effects on fibroblasts and ECM production. Many extracellular matrix proteins were increased by HSA treatment: Fibronectin type III domain-containing protein (FNDC1; 19.64X), vitronectin (VTN; 5.33X), hyaluronan-binding protein 2 (HABP2; 5.09X), proteoglycan 4 (PRG4; 2.91X), tenascin (TNC; 1.75X), matrilin-2 (MATN2; 1.47X), Versican core protein (VCAN; 1.38X), elasin microfibril interface 1 (EMILIN-1; 1.30X) and collagens alpha chain-2 & -3 (VI) (COL6A2/6A3; 1.31 & 1.22 X) which will all help with strengthening the pore wall structure (Table III).

(R)-10-HSA is a transactivating ligand of PPAR α

In a transient transactivation assay both HSA forms (*R*-enantiomer and racemate) were tested for ligand binding and subsequent transactivation using human peroxisome proliferator-activated receptor proteins, PPAR α , PPAR β and PPAR γ . Only PPAR α was positive for HSA. The half-maximal effective (EC₅₀) concentration for the *R*-enantiomeric HSA was determined to be 5.43 \pm 0.18 μ M, whereas the racemate was 11.81 \pm 0.39 μ M indicating that only (*R*)-10-hydroxystearic acid and not the (*S*)-10-hydroxystearic acid is a PPAR α agonist (Table VI).

In silico mechanistic evidence for binding of HSA to PPAR α

Docking of HSA into PPAR α revealed that the carboxylic acid moiety of HSA forms H-bonds with Tyr 314(H5), His440(H11) and Tyr464(H12) and Ser280 (H3), which also forms a H-bond to the hydroxy group in HSA (Fig. 6). This hydrogen bond network is key in stabilizing the active conformation of PPAR α required for heterodimerization with retinoid receptor (RXR) [24]. This heterodimer promotes coactivator recruitment that increases transcriptional activity [25].

Clinical effects of HSA reduced age spots and conspicuous pores

Conspicuous facial pores and age spots on healthy subjects were significantly reduced by a 1% (33 mM) HSA formulation compared to the vehicle treatment. The image analysis of both pore parameters, volume and surface, showed statistical significance ($p < 0.05$) of the product versus the vehicle treatment after 8 weeks of treatment (Fig. 7 & 8). Age spots became significantly lighter than the surrounding skin by product compared to vehicle application when analyzing contrast by the differences in ITA $^{\circ}$ angles between the surroundings and the pigmented spot after 4 weeks of treatment (Fig. 9 & 10).

Discussion.

Consumer research indicates that the expression of age spots and pores are of major concern to consumers globally. Both skin problems are induced by oxidative stress to the skin and have some similarities in their pathophysiology. Poor keratinocyte differentiation and aberrations to the DEJ are characteristic to both [5, 7, 17, 18, 26-29]. As a result, agents that improve epidermal differentiation or reduce the negative effects of UV irradiation on keratinocyte differentiation are likely to be beneficial. Proteases are also involved in their formation: MMPs are involved in the destruction of the dermal matrix in conspicuous pores and ADAMs, a type of MMP, induce melanogenesis [6, 30]. Consequently, agents that reduce the levels of MMPs will be advantageous. Moreover, agents known to improve the levels of collagen will likely counteract the pilosebaceous pore wall slackening that occurs in conspicuous pores. In addition, paracrine signalling molecules induced by UV irradiation on keratinocytes and fibroblasts induce melanogenesis [16, 17]. Also, the effects of UV on increasing sebaceous gland activity should not be underestimated in the expression of skin pores also [31]. Here we identified the monohydroxy fatty acid HSA to counteract many of these issues and to reduce facial age spots and conspicuous pores *in vivo*. In this respect improvements in reduction of conspicuous skin pores and age spots were observed as early as 4 weeks clinically, although the effect of HSA on age spots was slightly less at 8 weeks.

To clarify mechanisms of action several *in vitro*, *ex vivo* and *in silico* studies were performed. HSA was shown to reduce the negative effects of UV irradiation on the epidermis *in vitro* (reduced sunburn cell formation and p53 levels). These effects are consistent with an improvement in keratinocyte differentiation capacity and will help with the poor keratinization of keratinocytes in age spots and the surrounding epidermis around skin pores [17-19]. Furthermore, HSA was also shown to increase

collagen type I & III synthesis and reduce MMP levels which will help to improve the pilosebaceous pore wall slackening in conspicuous skin pores. Relatively higher increases in collagen type III are indicative of extracellular matrix remodelling and a more 'youthful' dermis [32]. Moreover, reducing the negative effect of UV on melanogenesis will aid the reduction in expression of age spots.

In an attempt to provide greater insight into the potential mechanism of action of HSA, particularly on the potential paracrine effect of fibroblasts after treatment, on the expression of pore and age spot problems we examined changes in secretome of fibroblasts (cell culture conditioned media), determined by mass spectrometry-based proteomics, that might influence the fibroblasts in autocrine fashion or keratinocytes or melanocytes in a paracrine fashion [15, 16]. Dermal fibroblasts play a key role in ECM formation and melanocyte pigmentation [33, 34]. Naturally our analysis excludes the impact of the role of other cells in skin.

352 secreted proteins were annotated. However, first we need to consider gene and protein expression in age spots (and related disorders) and determine if we observe and relatable changes in our fibroblast secretome dataset. The regulation of genes associated with the WNT signaling pathways have been described in age spots as well as melasma. Increased sFRP-1 and FRZB/sFRP3 together with increased WNT1, WNT5a and Frizzled-4 expression were found in age spots [35-37], whereas increased WNT expression increases in WIF1, sFRP2 and WNT5a were observed in melasma [38, 39]. We observed decreased levels of sFRP-1 and DKK1 indicating that changes in at least the former of these fibroblast proteins induced by HSA have the potential to reduce melanogenesis and age spot expression. Others that may act via the WNT signaling pathway are IGFBP2 and ANGPTL4 which are both reported to be WNT antagonists by inhibiting lipoprotein receptor-related protein 6 [40, 41]. In respect of the former molecule, IGF-1 is reported to be melanogenic and IGFBP2 might also control melanogenesis by reducing its unbound levels [42]. Adrenomedullin, which was also decreased following HSA treatment, is also a WNT signaling inhibitor and a melanocyte dendritic branching factor and may therefore decrease melanogenesis [43, 44]. The increased levels of Semaphorin 3A may also contribute as it is reported to decrease melanoma motility, invasiveness and proliferation [45]. The reductions in Netrin-1 and FGF5 may also contribute to decreased expression of age spots as they decrease melanocyte migration [46, 47]. As we observed a decreased age spot expression clinically following HSA treatment these changes *in vitro* must override any positive effects on melanocytes induced by Cyr61 and DKK [48, 49].

Concerning conspicuous pores, the IGF/IGFBP pathway appears to be altered [50, 51]. Increased levels of free IGF-1 can lead to disturbances in the architecture of the DEJ, pore wall slackening, increased sebum production and hyperproliferation of keratinocytes. IGFBP-3 is a major IGF binding protein and its loss in the rete ridges leads to keratinocyte hyperproliferation and the associated alterations in the DEJ. Interestingly, its levels are normal at the tips of the dermal papillae. Increased levels of K16 were observed in the conspicuous pores. A small decrease in IGFBP3 was observed in

our HSA-treated fibroblast secretome, however, the much larger increases in IGFBP2 may mitigate the negative effects of IGF-1 on the expression of conspicuous pores [52].

Moreover, midkine is known to influence keratinocyte differentiation being expressed before transglutaminase-1 [53]. ANGPTL4 which was also dramatically increased by HSA treatment is known to also mediate keratinocyte differentiation [54]. BIGH3 also increases keratinocyte differentiation [55]. Levels of semaphorin 3A were also increased that may contribute to the reduction of skin pores by reducing keratinocyte hyperproliferation in the rete ridges via its receptor neuropilin-1 [56]. Via this mechanism it may also prevent UV-induced apoptosis and expression of p53 [57]. Adrenomedullin also increases keratinocyte proliferation and its reduced levels may also have a positive benefit [58]. Conversely, we found increased levels of SDF-1 which is known to promote keratinocyte hyperproliferation and we believe its likely effects are counteracted by all the above other changes in other proteins [59].

Improving ECM production is also key in strengthening pore walls to alleviate the expression of conspicuous pores. Of the factors already discussed BIGH3 promotes the function of fibroblasts interacting with biglycan and decorin to promote collagen aggregation and ANGPTL4 enhances the proliferation and migration of fibroblasts [60-62]. Midkine also stimulates Collagen's I/III, glycosaminoglycan synthesis and especially hyaluronic acid and this may be reflected in the changes in collagen 6A2 & 6A3 levels and HABP2 levels in our samples [63]. Other proteins that are increased that will help are fibronectin type III repeats, vitronectin and proteoglycan 4 (lubricin) that promote migration of dermal fibroblasts [64-67]. PTX3 also promotes wound healing and fibrin remodeling [68]. The increases in tenascin, versican and matrilin-2 are also involved in ECM remodeling [69-71]. Moreover, during extracellular matrix assembly EMLINS, which we found to be increased, are deposited on and co-regulated with fibrillins [72]. LTBP2 is also enhanced in intrinsically aged skin reducing TGF β activity and its suppression in our samples may aid ECM production [73]. The increases in CYP61 are known to increase MMP-1 levels [74]. This might be considered to be negative for skin benefits, but all ECM remodeling requires turnover of the existing ECM [75]. The reduced levels of other proteins following HSA treatment are unclear (CD44, ELN, VIM, LMNA).

Several proteases are increased in solar lentigines and their suppression may aid both the increased melanogenesis and ECM destruction in both these and conspicuous pores. However, some may be involved in ECM remodeling. In this respect we found increases in prothrombin and ADAMTS1 that may be involved in fibroblast chemotaxis and migration while ADAMTS5 has a role to play in optimal versican content [76-80]. We also observed increases in the levels of HtrA1 which facilitates TGF β signaling by processing LTBP-1 [81]. Reduced MMP-14 may lead to increased ECM. The role of increased CPZ & PRSS23 together with decreased levels of THSD4, CAPN2 and sulphatase-1 are unknown in this respect.

Increased alpha-2-antiplasmin may help to mitigate plasmin destruction of the DEJ and activation of MMPs [82, 83]. The increased levels of antithrombin III may be to balance the (pro)thrombin activity [84]. TIMP-3 has the broadest MMP inhibition of all TIMP's and may mitigate excessive MMP proteolysis in the pore walls of conspicuous pores similarly increased levels of TFPI & ITIH2 may control other proteases [85-87]. The latter may also have a role to play in hyaluronic acid metabolism as it is a HABP. Serpin H1 (Hsp47) is a collagen-specific chaperone and the slight decline in its levels are uncertain but expression kinetics may have a role to play as previously discussed [88].

Some changes in protein levels were consistent with increased PPAR activity e.g. increased levels of ANGPTL4 and IGF/IGFBP responses [54, 89-91]. We focussed on PPAR α activity as we could not detect any activity in PPAR $\beta\delta\gamma$ in reporter gene assays (>15 μ M). Its EC₅₀ of 5.54 μ M for the enantiopure HSA was superior to the racemate and other HSA isomers. The *in silico* docking studies showed that the carboxylic acid moiety of HSA forms H-bonds with Tyr 314(H5), His440(H11) and Tyr464(H12) and Ser280 (H3) in the PPAR binding pocket, which also forms a H-bond to the hydroxy group in HSA [24]. This hydrogen bond network is key in stabilizing the active conformation of PPAR α required for heterodimerization with its partner the retinoid receptor (RXR) that is necessary for PPAR activity [25].

We believe targeting PPAR α to be important in targeting conspicuous pores and age spots as levels of its mRNA are diminished in photodamaged skin [92-94]. Moreover, its levels were diminished in irradiated fibroblasts. Wy14643, a PPAR α agonist, was also shown to limit procollagen diminution and MMP expression induced by UV-irradiation in human dermal fibroblasts and mouse skin consistent with our findings.

PPAR α agonists have, in particular, been shown to improve keratinocyte differentiation [95]. Clearly HSA can directly target the keratinocytes but changes in the fibroblast secretome that then influence keratinocytes in a paracrine fashion are clearly possible but still yet to be proven.

Although controversial, activators for PPAR α and γ are also reported to enhance or diminish melanogenesis [96-100]. However, the most recent evidence indicates a potential reduction in melanogenesis for PPAR α [101]. Moreover, it is reported that PPAR α expression is down regulated in other skin pigmentary disorders such as melasma [39]. Although we have not measured melanogenesis *in vitro* we anticipate such an effect from HSA as a direct PPAR α target in melanocytes and indirectly from its PPAR activity on the fibroblast and keratinocyte secretome as our clinical results were unequivocal. Studies are ongoing to determine the most important potential paracrine signalling molecules *in vitro*.

In conclusion, HSA is a novel fatty acid for use in cosmetic formulations that we believe binds to PPAR α to induce changes in skin cells, particularly fibroblasts, to mitigate the presence of conspicuous skin pores and age spots.

References.

1. Kligman AM. Early destructive effect of sunlight on human skin. *JAMA*. 1969;210(13):2377-80.
2. Krutmann J, Bouloc A, Sore G, Bernard BA, Passeron T. The skin aging exposome. *J Dermatol Sci*. 2017;85(3):152-61.
3. Flament F, Francois G, Qiu H, Ye C, Hanaya T, Batisse D, et al. Facial skin pores: a multiethnic study. *Clin Cosmet Investig Dermatol*. 2015;8:85-93.
4. Hillebrand G, Levine M, Miyamoto K. The age dependent changes in skin condition in African Americans, Asian Indians, Caucasians, East Asians and Latinos. *IFSCC Magazine*. 2001;4(4):259-66.
5. Sugiyama-Nakagiri Y, Sugata K, Hachiya A, Osanai O, Ohuchi A, Kitahara T. Ethnic differences in the structural properties of facial skin. *J Dermatol Sci*. 2009;53(2):135-9.
6. Lee SJ, Seok J, Jeong SY, Park KY, Li K, Seo SJ. Facial Pores: Definition, Causes, and Treatment Options. *Dermatol Surg*. 2016;42(3):277-85.
7. Katsuta Y, Iida T, Inomata S, Yoshida S. Improving the appearance of facial pores. *Cosmetics & Toiletries*. 2004;119(10):59-64.
8. Fink B, Matts PJ, Klingenberg H, Kuntze S, Weege B, Grammer K. Visual attention to variation in female facial skin color distribution. *J Cosmet Dermatol*. 2008;7(2):155-61.
9. Nkengne A, Bertin C, Stamatas GN, Giron A, Rossi A, Issachar N, et al. Influence of facial skin attributes on the perceived age of Caucasian women. *J Eur Acad Dermatol Venereol*. 2008;22(8):982-91.
10. Ortonne JP. Pigmentary changes of the ageing skin. *Br J Dermatol*. 1990;122 Suppl 35:21-8.
11. Ding A, Yang Y, Zhao Z, Huls A, Vierkotter A, Yuan Z, et al. Indoor PM2.5 exposure affects skin aging manifestation in a Chinese population. *Sci Rep*. 2017;7(1):15329.
12. Peng F, Xue CH, Hwang SK, Li WH, Chen Z, Zhang JZ. Exposure to fine particulate matter associated with senile lentigo in Chinese women: a cross-sectional study. *J Eur Acad Dermatol Venereol*. 2017;31(2):355-60.
13. Vierkotter A, Huls A, Yamamoto A, Stolz S, Kramer U, Matsui MS, et al. Extrinsic skin ageing in German, Chinese and Japanese women manifests differently in all three groups depending on ethnic background, age and anatomical site. *J Dermatol Sci*. 2016;83(3):219-25.
14. Joly-Tonetti N, Wibawa JID, Bell M, Tobin DJ. An explanation for the mysterious distribution of melanin in human skin: a rare example of asymmetric (melanin) organelle distribution during mitosis of basal layer progenitor keratinocytes. *Br J Dermatol*. 2018;179(5):1115-26.
15. Yuan XH, Jin ZH. Paracrine regulation of melanogenesis. *Br J Dermatol*. 2018;178(3):632-9.
16. Wang Y, Viennet C, Robin S, Berthon JY, He L, Humbert P. Precise role of dermal fibroblasts on melanocyte pigmentation. *J Dermatol Sci*. 2017;88(2):159-66.
17. Aoki H, Moro O, Tagami H, Kishimoto J. Gene expression profiling analysis of solar lentigo in relation to immunohistochemical characteristics. *Br J Dermatol*. 2007;156(6):1214-23.
18. Choi W, Yin L, Smuda C, Batzer J, Hearing VJ, Kolbe L. Molecular and histological characterization of age spots. *Exp Dermatol*. 2017;26(3):242-8.
19. Cottle DL, Kretzschmar K, Gollnick HP, Quist SR. p53 activity contributes to defective interfollicular epidermal differentiation in hyperproliferative murine skin. *Br J Dermatol*. 2016;174(1):204-8.
20. Todorovic V, Desai BV, Eigenheer RA, Yin T, Amargo EV, Mrksich M, et al. Detection of differentially expressed basal cell proteins by mass spectrometry. *Molecular & cellular proteomics : MCP*. 2010;9(2):351-61.
21. Voegeli R, Monneuse JM, Schoop R, Summers B, Rawlings AV. The effect of photodamage on the female Caucasian facial stratum corneum corneome using mass spectrometry-based proteomics. *International journal of cosmetic science*. 2017;39(6):637-52.
22. Gillet LC, Navarro P, Tate S, Rost H, Selevsek N, Reiter L, et al. Targeted data extraction of the MS/MS spectra generated by data-independent acquisition: a new concept for consistent and accurate proteome analysis. *Molecular & cellular proteomics : MCP*. 2012;11(6):O111.016717.

23. Singh SK, Abbas WA, Tobin DJ. Bone morphogenetic proteins differentially regulate pigmentation in human skin cells. *Journal of cell science*. 2012;125(Pt 18):4306-19.
24. Nolte RT, Wisely GB, Westin S, Cobb JE, Lambert MH, Kurokawa R, et al. Ligand binding and co-activator assembly of the peroxisome proliferator-activated receptor-gamma. *Nature*. 1998;395(6698):137-43.
25. Kota BP, Huang TH, Roufogalis BD. An overview on biological mechanisms of PPARs. *Pharmacol Res*. 2005;51(2):85-94.
26. Masuda Y, Oguri M, Morinaga T, Hirao T. Three-dimensional morphological characterization of the skin surface micro-topography using a skin replica and changes with age. *Skin Res Technol*. 2014;20(3):299-306.
27. Mizukoshi K, Yonekura K, Futagawa M, Nakamura T, Hirayama K, Takahashi K. Changes in dermal papilla structures due to aging in the facial cheek region. *Skin Res Technol*. 2015;21(2):224-31.
28. Pollefliet C, Corstjens H, Gonzalez S, Hellemans L, Declercq L, Yarosh D. Morphological characterization of solar lentigines by in vivo reflectance confocal microscopy: a longitudinal approach. *International journal of cosmetic science*. 2013;35(2):149-55.
29. Sugata K, Nishijima T, Kitahara T, Takema Y. Confocal laser microscopic imaging of conspicuous facial pores in vivo: relation between the appearance and the internal structure of skin. *Skin Res Technol*. 2008;14(2):208-12.
30. Kawaguchi M, Hozumi Y, Suzuki T. ADAM protease inhibitors reduce melanogenesis by regulating PMEL17 processing in human melanocytes. *J Dermatol Sci*. 2015;78(2):133-42.
31. Suh DH, Kwon TE, Youn JI. Changes of comedonal cytokines and sebum secretion after UV irradiation in acne patients. *Eur J Dermatol*. 2002;12(2):139-44.
32. Wang C, Rong Y, Ning F, Zhang G. The content and ratio of type I and III collagen in skin differ with age and injury. *Afric J Biotech*. 2011;10(13):2524-9.
33. Cole MA, Quan T, Voorhees JJ, Fisher GJ. Extracellular matrix regulation of fibroblast function: redefining our perspective on skin aging. *J Cell Commun Signal*. 2018;12(1):35-43.
34. Duval C, Cohen C, Chagnoleau C, Flouret V, Bourreau E, Bernerd F. Key regulatory role of dermal fibroblasts in pigmentation as demonstrated using a reconstructed skin model: impact of photo-aging. *PLoS One*. 2014;9(12):e114182.
35. Goyarts E, Muizzuddin N, Maes D, Giacomoni PU. Morphological changes associated with aging: age spots and the microinflammatory model of skin aging. *Ann N Y Acad Sci*. 2007;1119:32-9.
36. Yamada T, Hasegawa S, Inoue Y, Date Y, Arima M, Yagami A, et al. Comprehensive analysis of melanogenesis and proliferation potential of melanocyte lineage in solar lentigines. *J Dermatol Sci*. 2014;73(3):251-7.
37. Yamada T, Hasegawa S, Inoue Y, Date Y, Arima M, Yagami A, et al. Accelerated differentiation of melanocyte stem cells contributes to the formation of hyperpigmented maculae. *Exp Dermatol*. 2014;23(9):652-8.
38. Esposito ACC, Brianezi G, de Souza NP, Miot LDB, Marques MEA, Miot HA. Exploring pathways for sustained melanogenesis in facial melasma: an immunofluorescence study. *International journal of cosmetic science*. 2018.
39. Kang HY, Suzuki I, Lee DJ, Ha J, Reiniche P, Aubert J, et al. Transcriptional profiling shows altered expression of wnt pathway- and lipid metabolism-related genes as well as melanogenesis-related genes in melasma. *J Invest Dermatol*. 2011;131(8):1692-700.
40. Cruciat CM, Niehrs C. Secreted and transmembrane wnt inhibitors and activators. *Cold Spring Harb Perspect Biol*. 2013;5(3):a015081.
41. Kirsch N, Chang LS, Koch S, Glinka A, Dolde C, Colozza G, et al. Angiopoietin-like 4 Is a Wnt Signaling Antagonist that Promotes LRP6 Turnover. *Dev Cell*. 2017;43(1):71-82 e6.
42. Hu S, Liu Y, Yang S, Ji K, Liu X, Zhang J, et al. The effects of IGF1 on the melanogenesis in alpaca melanocytes in vitro. *In Vitro Cell Dev Biol Anim*. 2016;52(8):806-11.
43. Lausson S, Cressent M. Signal transduction pathways mediating the effect of adrenomedullin on osteoblast survival. *J Cell Biochem*. 2011;112(12):3807-15.
44. Motokawa T, Miwa T, Mochizuki M, Toritsuka M, Sakata A, Ito M. Adrenomedullin: A novel melanocyte dendrite branching factor. *J Dermatol Sci*. 2015;79(3):307-10.
45. Chakraborty G, Kumar S, Mishra R, Patil TV, Kundu GC. Semaphorin 3A suppresses tumor growth and metastasis in mice melanoma model. *PLoS One*. 2012;7(3):e33633.
46. Ghassemi S, Vejdovsky K, Sahin E, Ratzinger L, Schelch K, Mohr T, et al. FGF5 is expressed in melanoma and enhances malignancy in vitro and in vivo. *Oncotarget*. 2017;8(50):87750-62.

47. Kaufmann S, Kuphal S, Schubert T, Bosserhoff AK. Functional implication of Netrin expression in malignant melanoma. *Cell Oncol.* 2009;31(6):415-22.
48. Xu Z, Chen L, Jiang M, Wang Q, Zhang C, Xiang LF. CCN1/Cyr61 Stimulates Melanogenesis through Integrin alpha6beta1, p38 MAPK, and ERK1/2 Signaling Pathways in Human Epidermal Melanocytes. *J Invest Dermatol.* 2018;138(8):1825-33.
49. Yamaguchi Y, Passeron T, Hoashi T, Watabe H, Rouzaud F, Yasumoto K, et al. Dickkopf 1 (DKK1) regulates skin pigmentation and thickness by affecting Wnt/beta-catenin signaling in keratinocytes. *FASEB J.* 2008;22(4):1009-20.
50. Sugiyama-Nakagiri Y, Naoe A, Ohuchi A, Kitahara T. Serum levels of IGF-1 are related to human skin characteristics including the conspicuousness of facial pores. *International journal of cosmetic science.* 2011;33(2):144-9.
51. Sugiyama-Nakagiri Y, Ohuchi A, Hachiya A, Kitahara T. Involvement of IGF-1/IGFBP-3 signaling on the conspicuousness of facial pores. *Arch Dermatol Res.* 2010;302(9):661-7.
52. Clemmons DR. IGF binding proteins and their functions. *Mol Reprod Dev.* 1993;35(4):368-74; discussion 74-5.
53. Monma F, Hozumi Y, Ikematsu S, Kawaguchi M, Kadomatsu K, Suzuki T. Expression of midkine in normal human skin, dermatitis and neoplasms: association with differentiation of keratinocytes. *J Dermatol.* 2013;40(12):980-6.
54. Pal M, Tan MJ, Huang RL, Goh YY, Wang XL, Tang MB, et al. Angiopoietin-like 4 regulates epidermal differentiation. *PLoS One.* 2011;6(9):e25377.
55. Oh JE, Kook JK, Min BM. Beta ig-h3 induces keratinocyte differentiation via modulation of involucrin and transglutaminase expression through the integrin alpha3beta1 and the phosphatidylinositol 3-kinase/Akt signaling pathway. *J Biol Chem.* 2005;280(22):21629-37.
56. Kurschat P, Bielenberg D, Rossignol-Tallandier M, Stahl A, Klagsbrun M. Neuron restrictive silencer factor NRSF/REST is a transcriptional repressor of neuropilin-1 and diminishes the ability of semaphorin 3A to inhibit keratinocyte migration. *J Biol Chem.* 2006;281(5):2721-9.
57. Riese A, Eilert Y, Meyer Y, Arin M, Baron JM, Eming S, et al. Epidermal expression of neuropilin 1 protects murine keratinocytes from UVB-induced apoptosis. *PLoS One.* 2012;7(12):e50944.
58. Albertin G, Carraro G, Parnigotto PP, Conconi MT, Ziolkowska A, Malendowicz LK, et al. Human skin keratinocytes and fibroblasts express adrenomedullin and its receptors, and adrenomedullin enhances their growth in vitro by stimulating proliferation and inhibiting apoptosis. *Int J Mol Med.* 2003;11(5):635-9.
59. Quan C, Cho MK, Shao Y, Miannecki LE, Liao E, Perry D, et al. Dermal fibroblast expression of stromal cell-derived factor-1 (SDF-1) promotes epidermal keratinocyte proliferation in normal and diseased skin. *Protein Cell.* 2015;6(12):890-903.
60. LeBaron RG, Bezverkov KI, Zimmer MP, Pavelec R, Skonier J, Purchio AF. Beta IG-H3, a novel secretory protein inducible by transforming growth factor-beta, is present in normal skin and promotes the adhesion and spreading of dermal fibroblasts in vitro. *J Invest Dermatol.* 1995;104(5):844-9.
61. Reinboth B, Thomas J, Hanssen E, Gibson MA. Beta ig-h3 interacts directly with biglycan and decorin, promotes collagen VI aggregation, and participates in ternary complexing with these macromolecules. *J Biol Chem.* 2006;281(12):7816-24.
62. Jamil S, Mousavizadeh R, Roshan-Moniri M, Tebbutt SJ, McCormack RG, Duronio V, et al. Angiopoietin-like 4 Enhances the Proliferation and Migration of Tendon Fibroblasts. *Med Sci Sports Exerc.* 2017;49(9):1769-77.
63. Yamada H, Inazumi T, Tajima S, Muramatsu H, Muramatsu T. Stimulation of collagen expression and glycosaminoglycan synthesis by midkine in human skin fibroblasts. *Arch Dermatol Res.* 1997;289(7):429-33.
64. Hintner H, Dahlback K, Dahlback B, Pepys MB, Breathnach SM. Tissue vitronectin in normal adult human dermis is non-covalently bound to elastic tissue. *J Invest Dermatol.* 1991;96(5):747-53.
65. Miyamoto Y, Tanabe M, Date K, Sakuda K, Sano K, Ogawa H. Sialylation of vitronectin regulates stress fiber formation and cell spreading of dermal fibroblasts via a heparin-binding site. *Glycoconj J.* 2016;33(2):227-36.
66. Obara M, Sakuma T, Fujikawa K. The third type III module of human fibronectin mediates cell adhesion and migration. *J Biochem.* 2010;147(3):327-35.
67. Sun Y, Berger EJ, Zhao C, Jay GD, An KN, Amadio PC. Expression and mapping of lubricin in canine flexor tendon. *J Orthop Res.* 2006;24(9):1861-8.

68. Cappuzzello C, Doni A, Dander E, Pasqualini F, Nebuloni M, Bottazzi B, et al. Mesenchymal Stromal Cell-Derived PTX3 Promotes Wound Healing via Fibrin Remodeling. *J Invest Dermatol.* 2016;136(1):293-300.
69. Bernstein EF, Fisher LW, Li K, LeBaron RG, Tan EM, Uitto J. Differential expression of the versican and decorin genes in photoaged and sun-protected skin. Comparison by immunohistochemical and northern analyses. *Lab Invest.* 1995;72(6):662-9.
70. Halper J, Kjaer M. Basic components of connective tissues and extracellular matrix: elastin, fibrillin, fibulins, fibrinogen, fibronectin, laminin, tenascins and thrombospondins. *Adv Exp Med Biol.* 2014;802:31-47.
71. Korpos E, Deak F, Kiss I. Matrilin-2, an extracellular adaptor protein, is needed for the regeneration of muscle, nerve and other tissues. *Neural Regen Res.* 2015;10(6):866-9.
72. Schiavinato A, Keene DR, Wohl AP, Corallo D, Colombatti A, Wagener R, et al. Targeting of EMILIN-1 and EMILIN-2 to Fibrillin Microfibrils Facilitates their Incorporation into the Extracellular Matrix. *J Invest Dermatol.* 2016;136(6):1150-60.
73. Langton AK, Sherratt MJ, Griffiths CE, Watson RE. Differential expression of elastic fibre components in intrinsically aged skin. *Biogerontology.* 2012;13(1):37-48.
74. Qin Z, Fisher GJ, Quan T. Cysteine-rich protein 61 (CCN1) domain-specific stimulation of matrix metalloproteinase-1 expression through α V β 3 integrin in human skin fibroblasts. *J Biol Chem.* 2013;288(17):12386-94.
75. Karimipour DJ, Kang S, Johnson TM, Orringer JS, Hamilton T, Hammerberg C, et al. Microdermabrasion with and without aluminum oxide crystal abrasion: a comparative molecular analysis of dermal remodeling. *J Am Acad Dermatol.* 2006;54(3):405-10.
76. Artuc M, Hermes B, Algermissen B, Henz BM. Expression of prothrombin, thrombin and its receptors in human scars. *Exp Dermatol.* 2006;15(7):523-9.
77. Dawes KE, Gray AJ, Laurent GJ. Thrombin stimulates fibroblast chemotaxis and replication. *Eur J Cell Biol.* 1993;61(1):126-30.
78. Hattori N, Carrino DA, Lauer ME, VasANJI A, Wylie JD, Nelson CM, et al. Pericellular versican regulates the fibroblast-myofibroblast transition: a role for ADAMTS5 protease-mediated proteolysis. *J Biol Chem.* 2011;286(39):34298-310.
79. Krampert M, Kuenzle S, Thai SN, Lee N, Iruela-Arispe ML, Werner S. ADAMTS1 proteinase is up-regulated in wounded skin and regulates migration of fibroblasts and endothelial cells. *J Biol Chem.* 2005;280(25):23844-52.
80. Mead TJ, Apte SS. ADAMTS proteins in human disorders. *Matrix Biol.* 2018;71-72:225-39.
81. Beaufort N, Scharrer E, Kremmer E, Lux V, Ehrmann M, Huber R, et al. Cerebral small vessel disease-related protease HtrA1 processes latent TGF- β binding protein 1 and facilitates TGF- β signaling. *Proc Natl Acad Sci U S A.* 2014;111(46):16496-501.
82. Amano S. Characterization and mechanisms of photoageing-related changes in skin. Damages of basement membrane and dermal structures. *Exp Dermatol.* 2016;25 Suppl 3:14-9.
83. Schaefer BM, Maier K, Eickhoff U, Bechtel M, Kramer MD. α 2-Antiplasmin and plasminogen activator inhibitors in healing human skin wounds. *Arch Dermatol Res.* 1996;288(3):122-8.
84. Lu Z, Wang F, Liang M. SerpinC1/Antithrombin III in kidney-related diseases. *Clin Sci (Lond).* 2017;131(9):823-31.
85. Bost F, Diarra-Mehrpour M, Martin JP. Inter-alpha-trypsin inhibitor proteoglycan family--a group of proteins binding and stabilizing the extracellular matrix. *Eur J Biochem.* 1998;252(3):339-46.
86. Brew K, Nagase H. The tissue inhibitors of metalloproteinases (TIMPs): an ancient family with structural and functional diversity. *Biochim Biophys Acta.* 2010;1803(1):55-71.
87. Papareddy P, Kalle M, Sorensen OE, Lundqvist K, Morgelin M, Malmsten M, et al. Tissue factor pathway inhibitor 2 is found in skin and its C-terminal region encodes for antibacterial activity. *PLoS One.* 2012;7(12):e52772.
88. Ito S, Nagata K. Biology of Hsp47 (SerpH1), a collagen-specific molecular chaperone. *Semin Cell Dev Biol.* 2017;62:142-51.
89. Kang HS, Kim MY, Kim SJ, Lee JH, Kim YD, Seo YK, et al. Regulation of IGF1BP2 expression during fasting. *Biochem J.* 2015;467(3):453-60.
90. McMullen PD, Bhattacharya S, Woods CG, Sun B, Yarborough K, Ross SM, et al. A map of the PPAR α transcription regulatory network for primary human hepatocytes. *Chem Biol Interact.* 2014;209:14-24.
91. Urbanska K, Pannizzo P, Grabacka M, Croul S, Del Valle L, Khalili K, et al. Activation of PPAR α inhibits IGF-I-mediated growth and survival responses in medulloblastoma cell lines. *Int J Cancer.* 2008;123(5):1015-24.

92. Kim EJ, Jin XJ, Kim YK, Oh IK, Kim JE, Park CH, et al. UV decreases the synthesis of free fatty acids and triglycerides in the epidermis of human skin in vivo, contributing to development of skin photoaging. *J Dermatol Sci*. 2010;57(1):19-26.
93. Shin MH, Lee SR, Kim MK, Shin CY, Lee DH, Chung JH. Activation of Peroxisome Proliferator-Activated Receptor Alpha Improves Aged and UV-Irradiated Skin by Catalase Induction. *PLoS One*. 2016;11(9):e0162628.
94. Xue J, Zhu W, Song J, Jiao Y, Luo J, Yu C, et al. Activation of PPARalpha by clofibrate sensitizes pancreatic cancer cells to radiation through the Wnt/beta-catenin pathway. *Oncogene*. 2018;37(7):953-62.
95. Hanley K, Jiang Y, He SS, Friedman M, Elias PM, Bikle DD, et al. Keratinocyte differentiation is stimulated by activators of the nuclear hormone receptor PPARalpha. *J Invest Dermatol*. 1998;110(4):368-75.
96. Chen JH, Chang JL, Chen PR, Chuang YJ, Tang ST, Pan SF, et al. Inhibition of peroxisome proliferator-activated receptor gamma prevents the melanogenesis in murine B16/F10 melanoma cells. *Biomed Res Int*. 2014;2014:695797.
97. Flori E, Mastrofrancesco A, Kovacs D, Ramot Y, Briganti S, Bellei B, et al. 2,4,6-Octatrienoic acid is a novel promoter of melanogenesis and antioxidant defence in normal human melanocytes via PPAR-gamma activation. *Pigment Cell Melanoma Res*. 2011;24(4):618-30.
98. Huang YC, Liu KC, Chiou YL, Yang CH, Chen TH, Li TT, et al. Fenofibrate suppresses melanogenesis in B16-F10 melanoma cells via activation of the p38 mitogen-activated protein kinase pathway. *Chem Biol Interact*. 2013;205(3):157-64.
99. Kang HY, Chung E, Lee M, Cho Y, Kang WH. Expression and function of peroxisome proliferator-activated receptors in human melanocytes. *Br J Dermatol*. 2004;150(3):462-8.
100. Wiechers JW, Rawlings AV, Garcia C, Chesne C, Balaguer P, Nicolas JC, et al. A new mechanism of action for skin whitening agents: binding to the peroxisome proliferator-activated receptor. *International journal of cosmetic science*. 2005;27(2):123-32.
101. Grabacka M, Wieczorek J, Michalczyk-Wetula D, Malinowski M, Wolan N, Wojcik K, et al. Peroxisome proliferator-activated receptor alpha (PPARalpha) contributes to control of melanogenesis in B16 F10 melanoma cells. *Arch Dermatol Res*. 2017;309(3):141-57.

Legends.

Table I. INCI list of formulation (Vehicle is minus HSA and replaced by water)

Table II. Paracrine/Autocrine growth factors and cytokines that modulate keratinocyte differentiation & ECM production to influence pore wall elasticity and melanogenesis in age spots

Table III. Structural proteins of ECM and DEJ to influence pore wall elasticity and melanogenesis in age spots

Table IV. Proteases and sulphatases that degrade extracellular matrix and modulate melanogenesis via protease-activated receptors to influence pore wall elasticity and melanogenesis in age spots

Table V. Protease inhibitors to prevent ECM destruction and melanogenesis to influence pore wall elasticity and melanogenesis in age spots

Table VI. EC₅₀ values [μM] PPARα. PPARα agonist drug GW7647 was used as positive control. Chiral (R)-HSA was significantly different to the racemate (p<0.05).

Figure 1: Collagen type 1 (**A**) and type 3 (**B**) stimulation by HSA and TGF β (transforming growth factor beta 1) as positive control in primary human dermal fibroblasts. Mean values \pm SEM, n=3, * p<0.01 relative to medium control.

Figure 2. A) IHC staining for type 3 collagen in human *ex vivo* skin. Comparison of vehicle (DMSO) vs. HSA treatment (0.1% = 3.3 mM) at day 6. **B)** Quantification of type 3 collagen of IHC stained sections. Mean values \pm SEM, n=12, **p<0.01 significance relative to vehicle control.

Figure 3. Comparison of *ex vivo* treatments vs. vehicle (DMSO) 24 h after UVB irradiation. **A)** UVB-induced MMP-1 gene expression from skin sections by RT-qPCR. **B)** Sunburn cells quantification on H&E-stained skin sections. Mean values \pm SEM, n = 12; * p<0.05 vs. vehicle control (DMSO) + UVB.

Figure 4. A) IHC stained skin section for p53 analysis. **B)** Image analysis of p53-stained skin sections. Mean values \pm SEM, n = 12, ** p<0.01 significance vs. vehicle (DMSO) control.

Figure 5. Total number of proteins identified and % of proteins that were modulated by HSA and TGF-beta.

Figure 6. Molecular modelling of docking of HSA to PPAR α . Docking of 10- HSA (blue tubes) into PPAR α (PDB: 3SP6, shown in green).

Figure 7. Surface and volume differences of conspicuous pores for product and vehicle treatment compared to T=0. Mean \pm SEM; Mann-Whitney test, *significance p<0.05 Product vs Vehicle.

Figure 8. Reduction of conspicuous facial pores on subject #20 after treatment with product formulation (1% HSA). VISIA-CR images taken at T = 0, 4, and 8 weeks: Parallel-polarized photos and pore surface segmentation near the nose (as shown as in blue).

Figure 9. Left: Projection of pigmentation extent in age spot region: Age spot region becomes lighter than surroundings after treatment. **Right:** Contrast given by differences between ITA $^{\circ}$ values of surrounding skin and age spot for T=4 and 8 weeks compared to baseline. Three pigmented spots per subject were chosen from the profile with the largest area and best contrast. Mean \pm SEM; Student t-test *significance p<0.05 Product vs Vehicle.

Figure 10. Cross-polarized photos from selected pigment spot selected of subject #20 which was treated with product formulation (1 % HSA) at T=0, 4, and 8 weeks. Below images encoded along the projection axis using false colors for pigmentation.

Table I. INCI list of formulation (Vehicle is minus HSA and replaced by water).

AQUA, HOMOSALATE, ETHYLHEXYL SALICYLATE, C12-15 ALKYL BENZOATE, BUTYL METHOXYDIBENZOYLMETHANE, OCTOCRYLENE, STEARETH-2, BUTYLENE GLYCOL, CETEARYL ALCOHOL, HYDROXYSTEARIC ACID, STEARETH-21, PHENOXYETHANOL, ETHYLHEXYLGLYCERIN, XANTHAN GUM, BHT, ACRYLATES/C10-30 ALKYL ACRYLATE CROSSPOLYMER, DISODIUM EDTA, SODIUM HYDROXIDE.

Table II: Paracrine/Autocrine growth factors and cytokines that modulate keratinocyte differentiation & ECM production to influence pore wall elasticity and melanogenesis in age spots

Name	Gene names	Fold Change	p-value	Potential function
Midkine	MDK MK1 NEGF2	15.74	0.0027	Involved in keratinocyte differentiation
Insulin-like growth factor-binding protein 2	IGFBP2 BP2 IBP2	15.07	0.0001	insulin-like growth factor I binding to improve pores, reduce sebum, decrease fibroblast migration and decrease melanocyte growth.
Isoform Delta of Stromal cell-derived factor 1	CXCL12 SDF1 SDF1A SDF1B	3.94	0.0002	involved in melanocyte/fibroblast migration and keratinocyte proliferation. Enhances wound healing.
Angiopoietin-related protein 4	ANGPTL4 ARP4 HFARP PGAR PP1158 PSEC0166 UNQ171/PRO197	2.90	0.0004	wnt signalling antagonist to reduce melanogenesis. Also improves keratinocyte differentiation.
Connective tissue growth factor	CTGF CCN2 HCS24 IGFBP8	2.29	0.0001	insulin-like growth factor binding (as above). Increases procollagen production to help pore wall structure.
Protein CYR61	CYR61 CCN1 GIG1 IGFBP10	1.45	0.0007	extracellular matrix binding. Inhibits melanocyte growth but increases MMP's
Transforming growth factor-beta-induced protein ig-h3	TGFBI BIGH3	1.41	0.0000	promotes fibroblast growth and keratinocyte differentiation.
Semaphorin-3A	SEMA3A SEMAD	1.35	0.0332	inhibits inflammation (reduces melanogenesis and ECM destruction) and decreases TEWL (keratinocyte differentiation) via neuropilin-1 receptor that protects against UVB apoptosis.
Insulin-like growth factor-binding protein 3	IGFBP3 IBP3	0.90	0.0384	Increased levels in conspicuous pores
Growth/differentiation factor 15	GDF15 MIC1 PDF PLAB PTGFB	0.78	0.0078	transforming growth factor beta receptor binding [GO:0005160]. Involved in keratinocyte differentiation. GDF9 increases CTGF?
Dickkopf-related protein 1	DKK1 UNQ492/PRO1008	0.78	0.0050	low-density lipoprotein particle receptor antagonist activity and reduces melanogenesis
Secreted frizzled-related protein 1	SFRP1 FRP FRP1 SARP2	0.77	0.0050	frizzled binding reduces melanogenesis. Increased levels found in age spots

Fibroblast growth factor 5	FGF5	0.76	0.0483	fibroblast growth factor receptor binding and elevated levels in melanoma
Semaphorin-3B	SEMA3B SEMA5 SEMAA	0.72	0.0015	causes growth cone collapse of sensory neurons may help with itch
Netrin-1	NTN1 NTN1L	0.71	0.0329	proinflammatory and promotes melanoma invasiveness
Semaphorin-3D	SEMA3D UNQ760/PRO1491	0.63	0.0127	causes growth cone collapse of sensory neurons may help with itch
Gremlin-1	GREM1 CKTSF1B1 DAND2 DRM PIG2	0.48	0.0011	BMP binding and transient increases induces melanogenesis.
Adrenomedullin	ADM AM	0.36	0.0020	melanocyte dendrite branching factor, induces keratinocyte& fibroblast proliferation
Complement C1q tumor necrosis factor-related protein 3	C1QTNF3 CTRP3 UNQ753/PRO1484	0.34	0.0277	CTRP3 inhibits TGF- β 1 induced collagen synthesis, proliferation and migration. Attenuates CTGF production. CTRP3 also attenuated TGF- β 1-induced Smad3 phosphorylation, nuclear translocation, and interaction with p300

Table III: Structural proteins of ECM and DEJ to influence pore wall elasticity and melanogenesis in age spots

Fibronectin type III domain-containing protein 1	FNDC1 FNDC2 KIAA1866 MEL4B3	19.64	0.0000	ECM protein
Vitronectin	VTN	5.33	0.0000	extracellular matrix binding [GO:0050840]; heparin binding [GO:0008201]; integrin binding [GO:0005178]; polysaccharide binding [GO:0030247]; scavenger receptor activity [GO:0005044]
Hyaluronan-binding protein 2	HABP2 HGFAL PHBP	5.09	0.0345	glycosaminoglycan binding [GO:0005539]; serine-type endopeptidase activity [GO:0004252]
Proteoglycan 4	PRG4 MSF SZP	2.91	0.0290	polysaccharide binding [GO:0030247]; scavenger receptor activity [GO:0005044]
Pentraxin-related protein	PTX3 TNFAIP5 TSG14	1.93	0.0014	Involved in wound healing.
Tenascin	TNC HXB	1.75	0.0004	syndecan binding [GO:0045545]
Gremlin-2	GREM2 CKTSF1B2 DAND3 PRDC	1.74	0.0005	inhibits BMP signaling to reduce melanogenesis
Matrilin-2	MATN2 UNQ193/PRO219	1.47	0.0000	calcium ion binding [GO:0005509]
Versican core protein	VCAN CSPG2	1.38	0.0012	calcium ion binding [GO:0005509]; carbohydrate binding [GO:0030246]; extracellular matrix structural constituent [GO:0005201]; glycosaminoglycan binding [GO:0005539]; hyaluronic acid binding [GO:0005540]
Collagen alpha-2(VI) chain	COL6A2	1.31	0.0041	
EMILIN-1	EMILIN1 EMI	1.30	0.0001	extracellular matrix constituent conferring elasticity [GO:0030023]
Collagen alpha-3(VI) chain	COL6A3	1.22	0.0103	serine-type endopeptidase inhibitor activity [GO:0004867]
CD44 antigen	CD44 LHR MDU2 MDU3 MIC4	0.66	0.0066	collagen binding [GO:0005518]; hyaluronic acid binding [GO:0005540]; hyaluronan-glucosaminidase activity [GO:0004415]
Latent-transforming growth factor beta-binding protein 2	LTBP2 C14orf141 LTBP3	0.66	0.0007	Assists TGFbeta signaling for matrix production and melanogenesis
Collagen alpha-2(I) chain	COL1A2	0.59	0.0103	extracellular matrix structural constituent [GO:0005201]; identical protein binding [GO:0042802]; metal ion binding [GO:0046872]; platelet-derived growth factor binding [GO:0048407]; protein binding, bridging [GO:0030674]
Isoform 4 of Elastin	ELN	0.59	0.0018	extracellular matrix structural constituent [GO:0005201]
Vimentin	VIM	0.53	0.0002	double-stranded RNA binding [GO:0003725]; glycoprotein binding [GO:0001948]; identical protein binding [GO:0042802]; protein C-terminus binding [GO:0008022]; scaffold protein binding [GO:0097110]; structural constituent of cytoskeleton [GO:0005200]; structural constituent of eye lens [GO:0005212]
Prelamin-A/C	LMNA LMN1	0.06	0.0100	structural molecule activity [GO:0005198]

Table IV: Proteases and sulphatases that degrade extracellular matrix and modulate melanogenesis via protease-activated receptors to influence pore wall elasticity and melanogenesis in age spots.

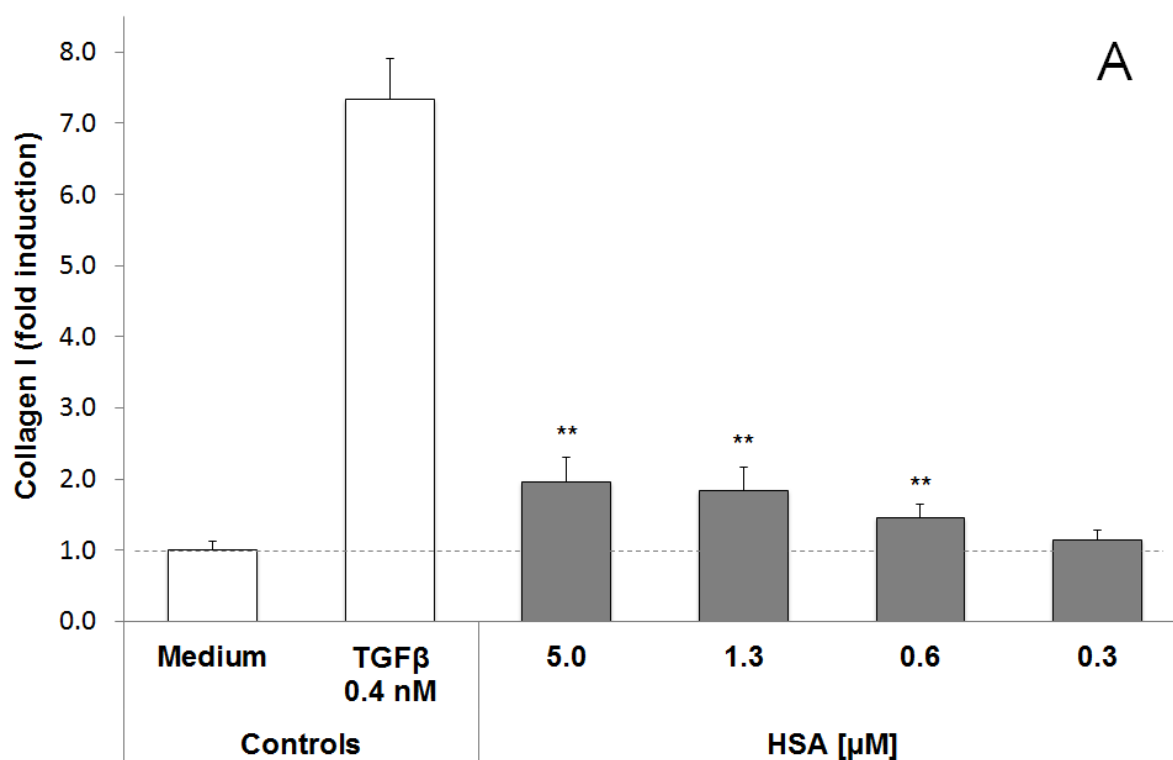
Prothrombin	F2	7.46	0.0000	serine-type endopeptidase activity
A disintegrin and metalloproteinase with thrombospondin motifs 1	ADAMTS1 KIAA1346 METH1	2.28	0.0064	metalloendopeptidase activity
A disintegrin and metalloproteinase with thrombospondin motifs 5	ADAMTS5 ADAMTS11 ADMP2	1.78	0.0134	metalloendopeptidase activity and modulates proteoglycan synthesis
Carboxypeptidase Z	CPZ	1.39	0.0232	metallocarboxypeptidase activity
Serine protease 23	PRSS23 ZSIG13 UNQ270/PRO307	1.35	0.0149	serine-type endopeptidase activity
Serine protease HTRA1	HTRA1 HTRA PRSS11	1.20	0.0033	serine-type endopeptidase. Regulates availability of IGF by cleaving IGFBP. Processes LTBP, facilitates TGFbeta signaling
Neurotrypsin	PRSS12	0.68	0.0250	serine-type endopeptidase activity
Matrix metalloproteinase-14	MMP14	0.65	0.0048	metalloendopeptidase activity
Extracellular sulfatase Sulf-1	SULF1 KIAA1077	0.65	0.0011	N-acetylglucosamine-6-sulfatase activity
Thrombospondin type-1 domain-containing protein 4	THSD4 UNQ9334/PRO34005	0.64	0.0055	metalloendopeptidase activity
Calpain-2 catalytic subunit	CAPN2 CANPL2	0.10	0.0038	calcium-dependent cysteine-type endopeptidase activity

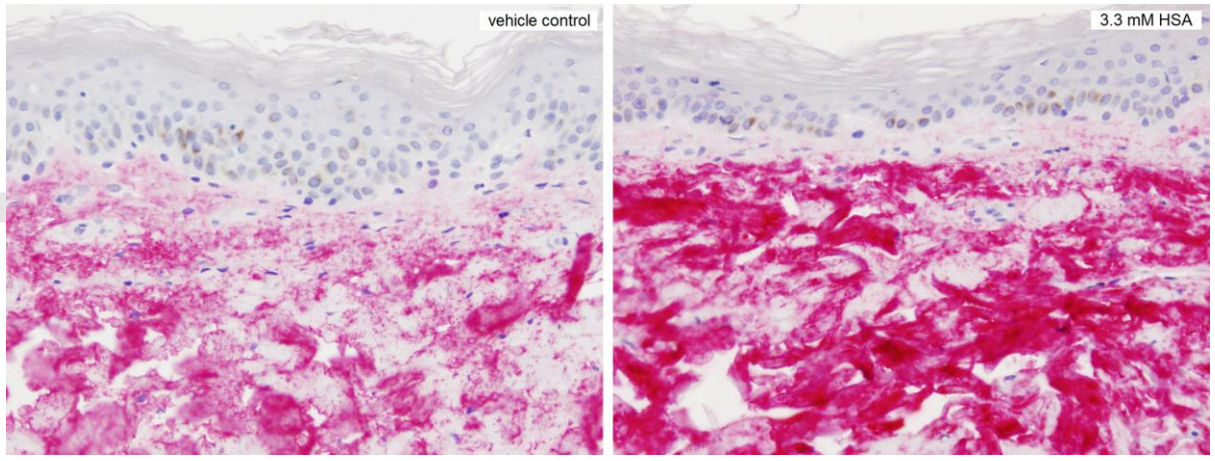
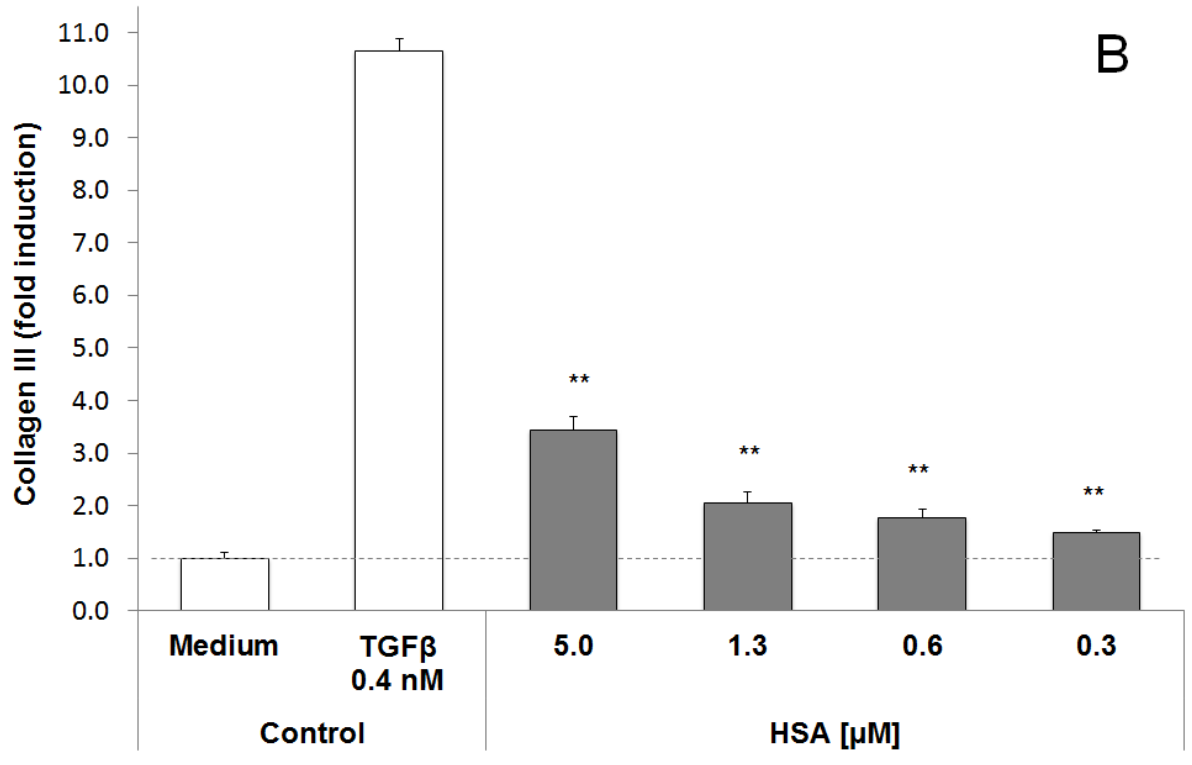
Table V: Protease inhibitors to prevent ECM destruction and melanogenesis to influence pore wall elasticity and melanogenesis in age spots

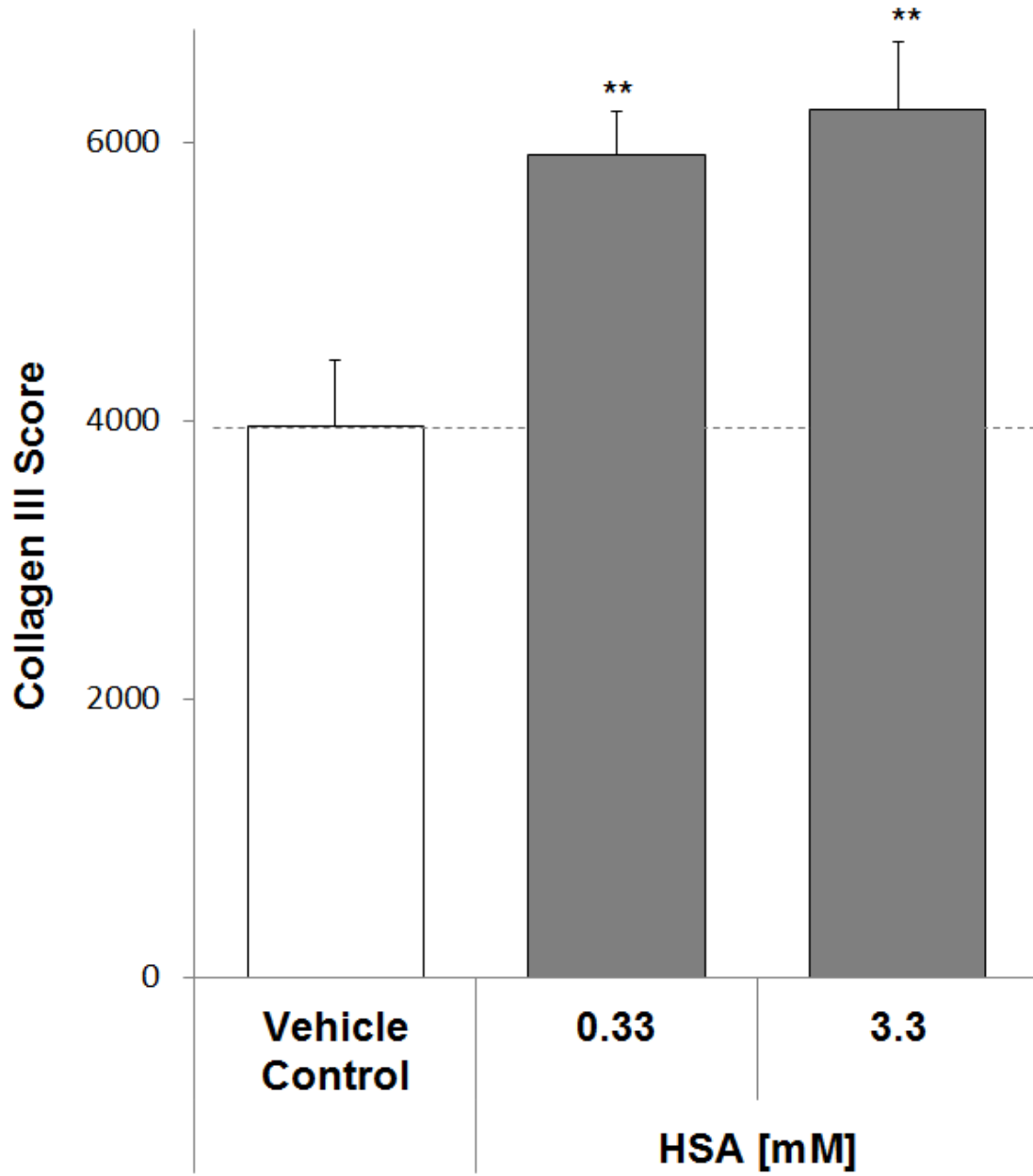
Alpha-2-antiplasmin	SERPINF2 AAP PLI	3.90	0.0202	serine-type endopeptidase inhibitor activity. Plasmin involved in age spot formation.
Antithrombin-III	SERPINC1 AT3 PRO0309	1.75	0.0029	serine-type endopeptidase inhibitor activity
Metalloproteinase inhibitor 3	TIMP3	1.66	0.0011	metalloendopeptidase inhibitor activity
Tissue factor pathway inhibitor	TFPI LACI TFPI1	1.55	0.0012	serine-type endopeptidase inhibitor activity
Inter-alpha-trypsin inhibitor heavy chain H2	ITIH2 IGHEP2	1.44	0.0020	serine-type endopeptidase inhibitor activity
Serpin H1	SERPINH1 CBP1 CBP2 HSP47 SERPINH2 PIG14	0.80	0.0266	serine-type endopeptidase inhibitor activity

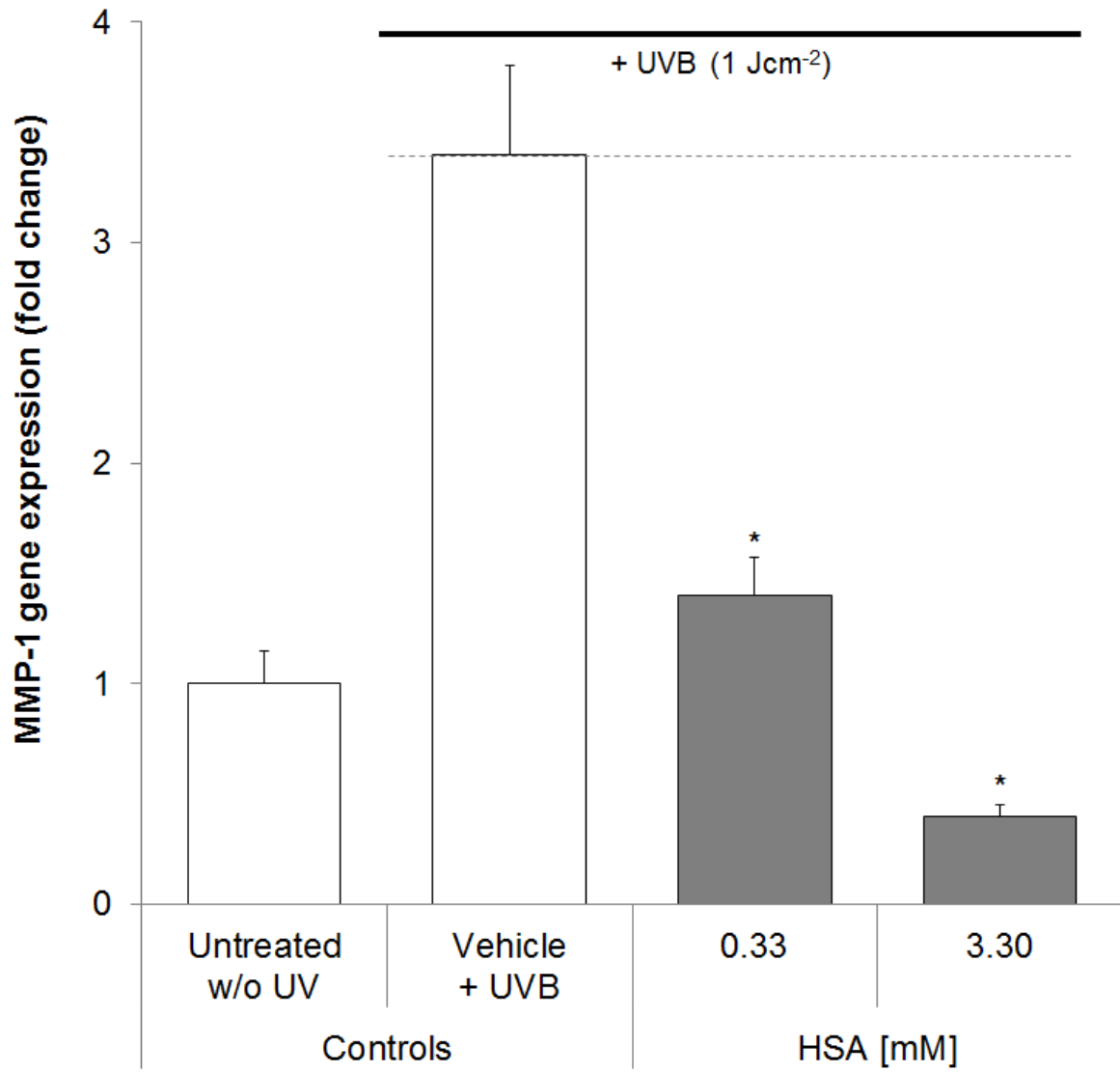
Table VI. EC₅₀ values [μM] PPARα. PPARα agonist drug GW7647 was used as positive control. Chiral (R)-HSA was significantly different to the racemate (p<0.05).

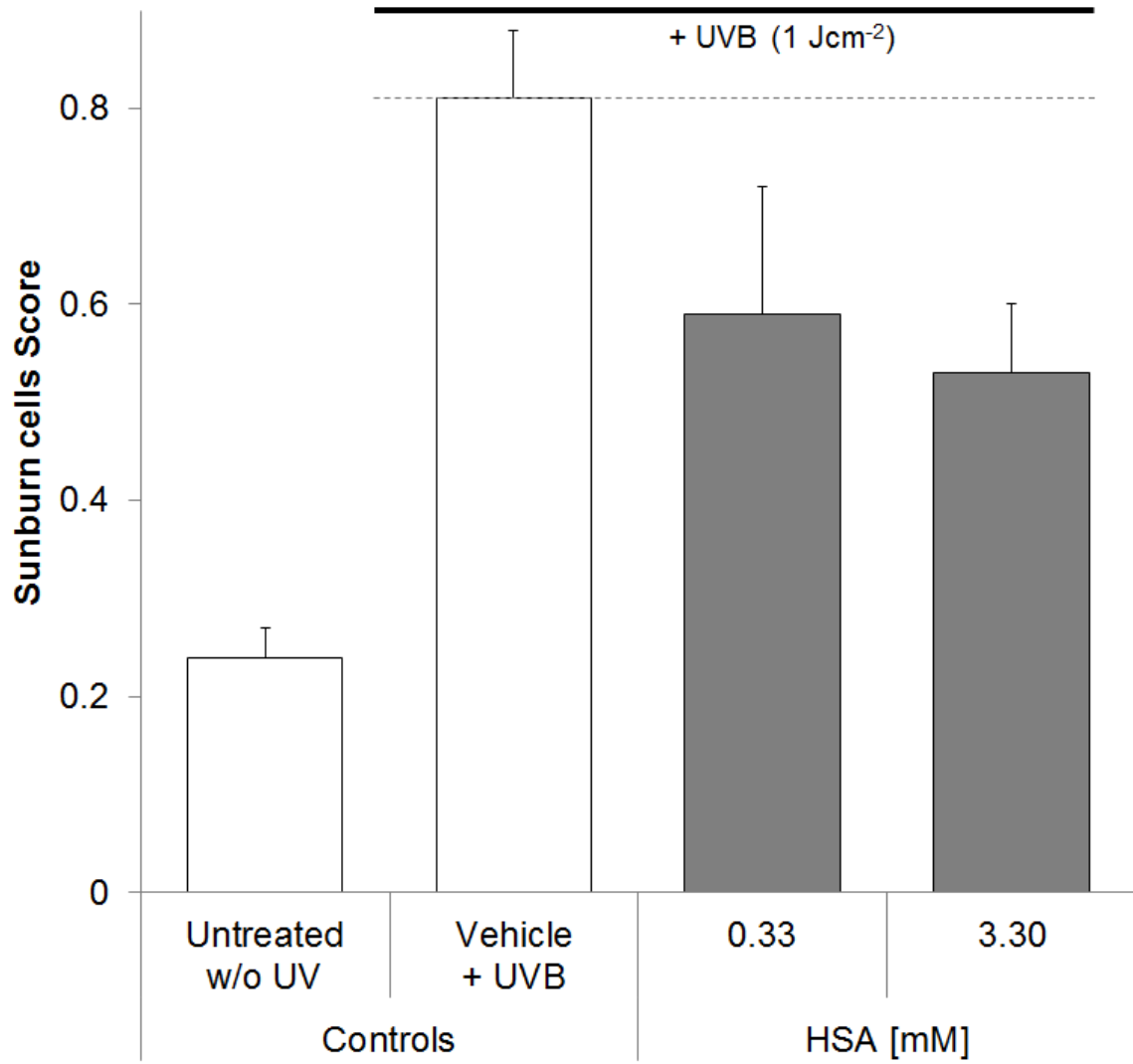
SUBSTANCE	EC ₅₀ [μM] PPARA	STD ERR	95% EC ₅₀ CONFIDENCE LIMITS [μM]
GW7647 (positive control, drug)	0.0119	±0.0006	[0.0106 – 0.0134]
(R)-10-Hydroxystearic acid (HSA)	5.4345	±0.1839	[5.0345 – 5.8670]
10-Hydroxystearic acid (RACEMATE)	11.8115	±0.3871	[10.9897 – 12.6947]

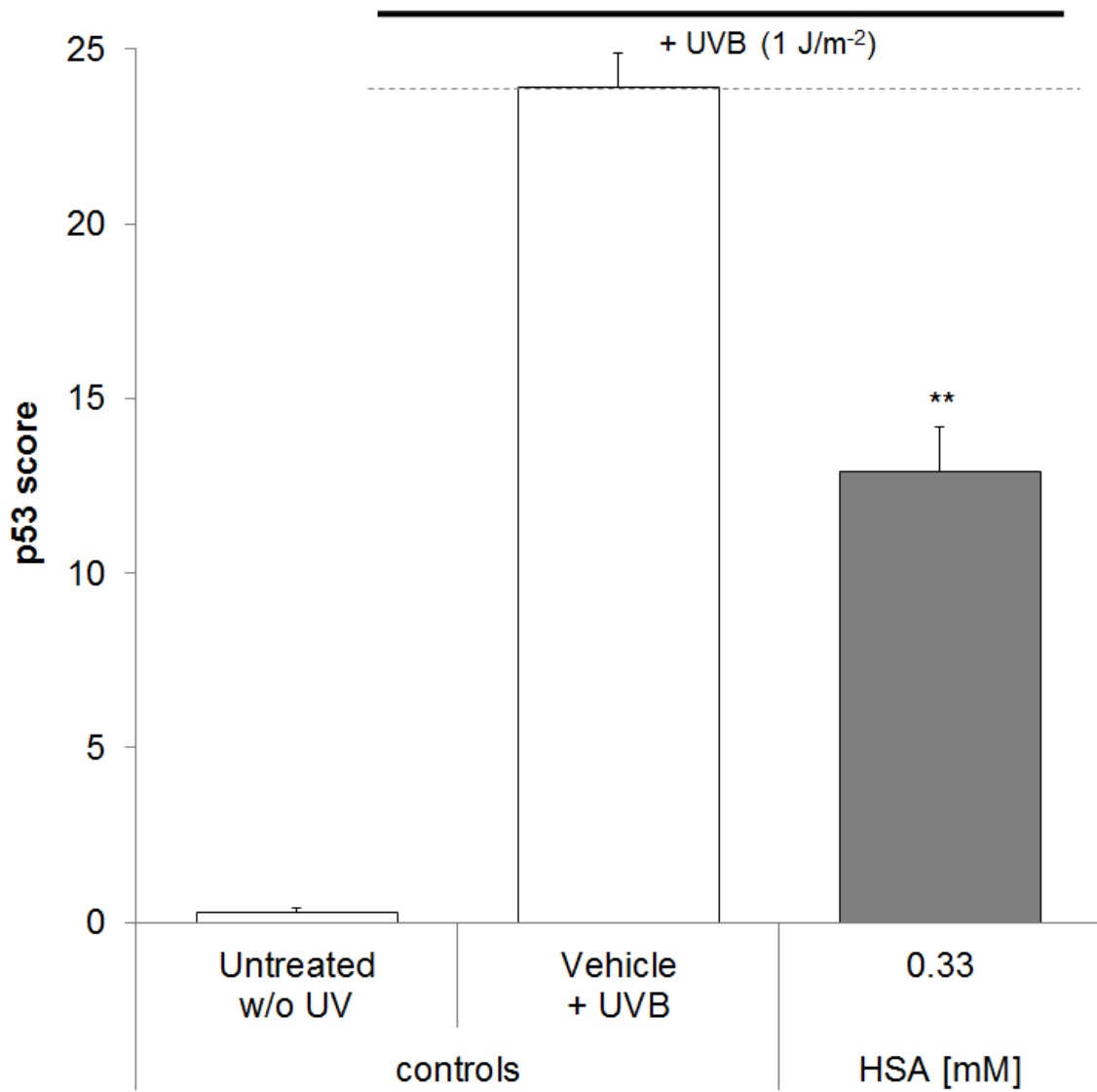
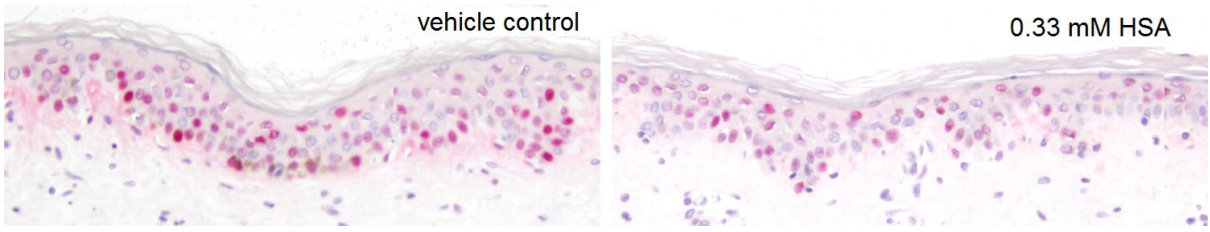


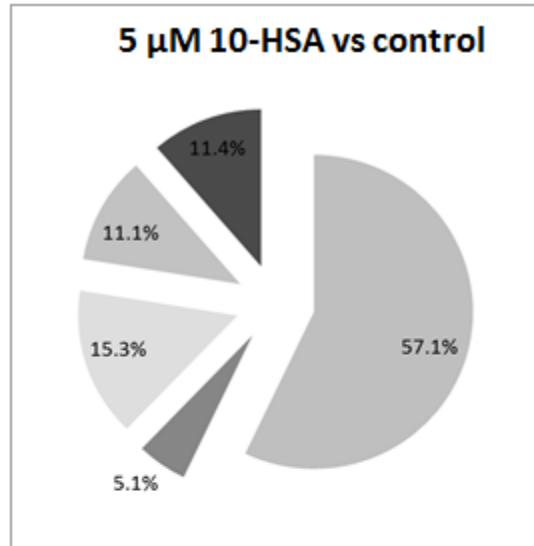
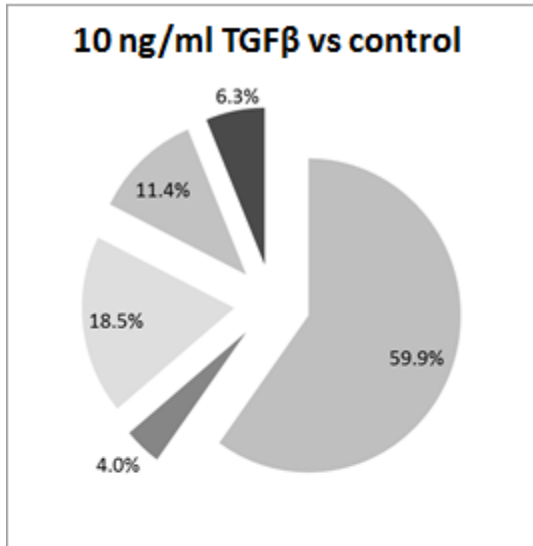




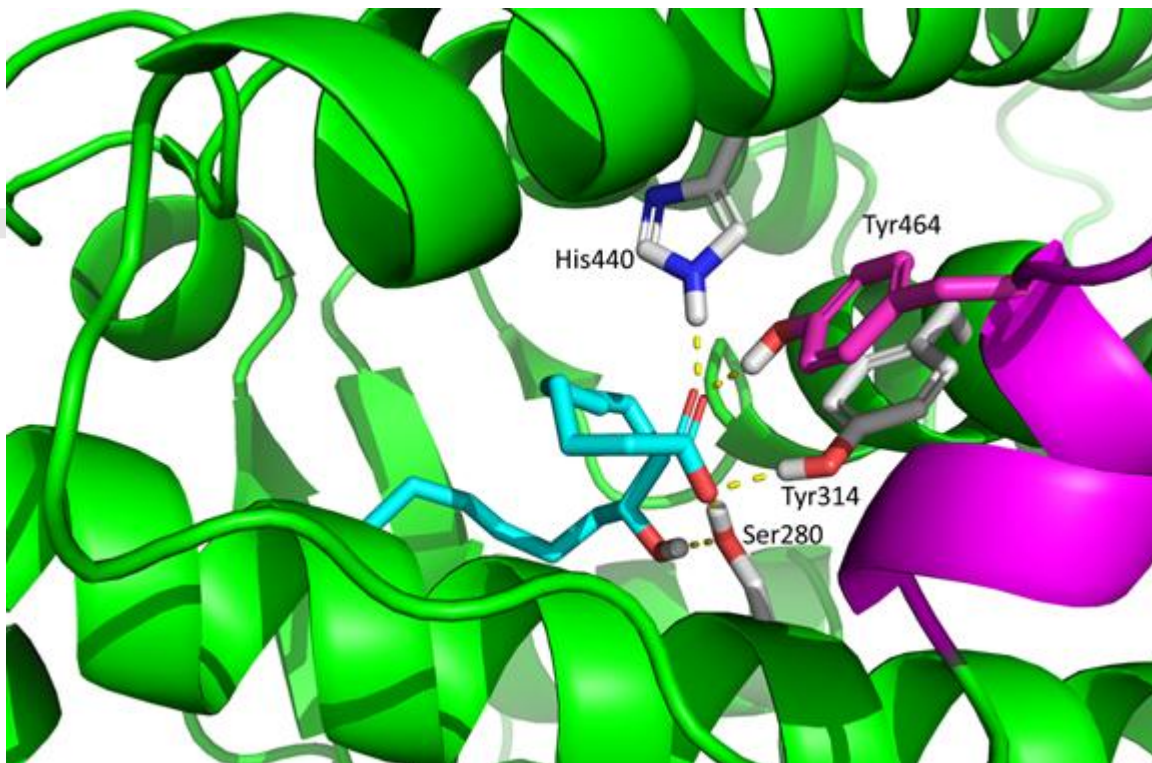


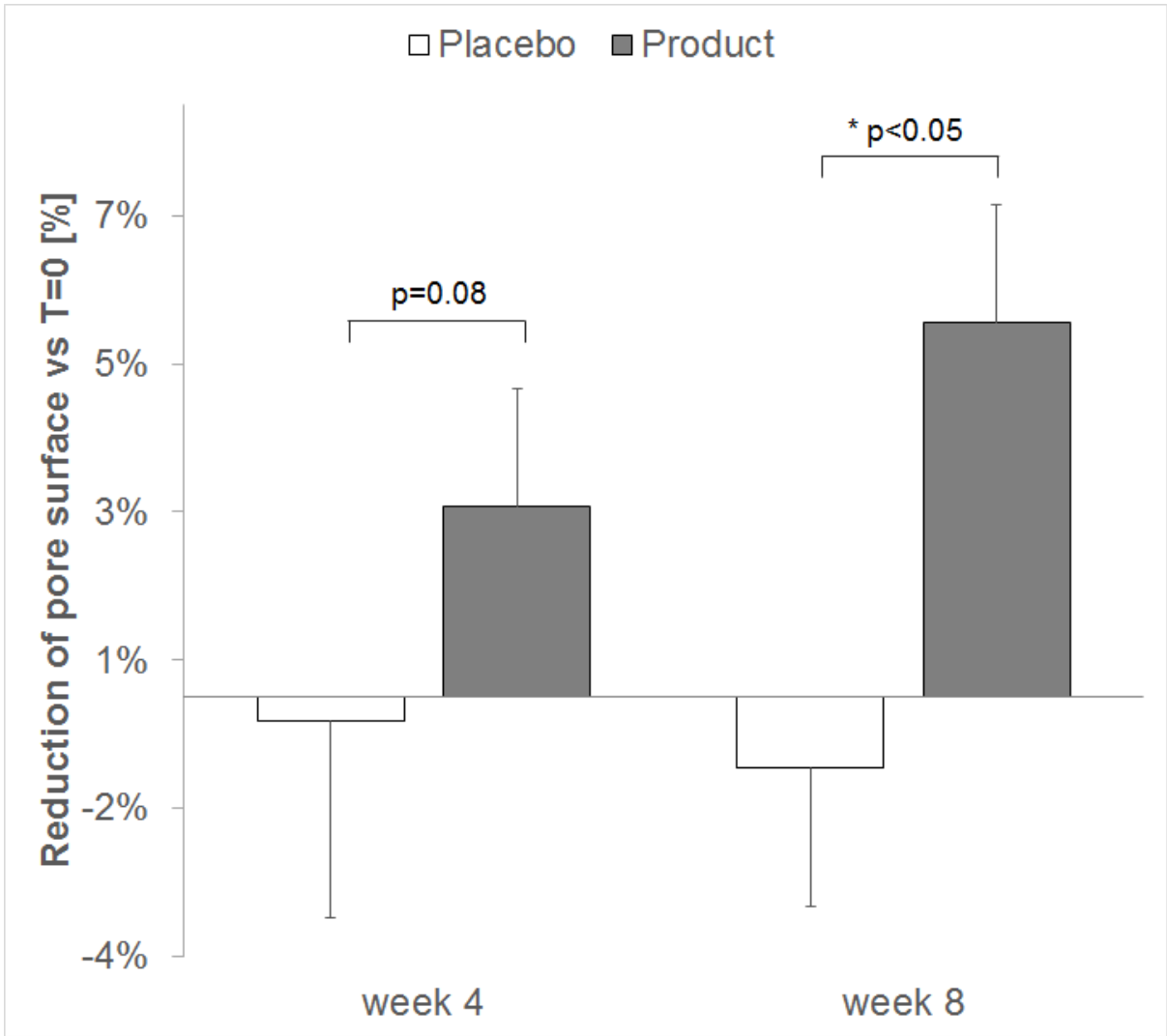


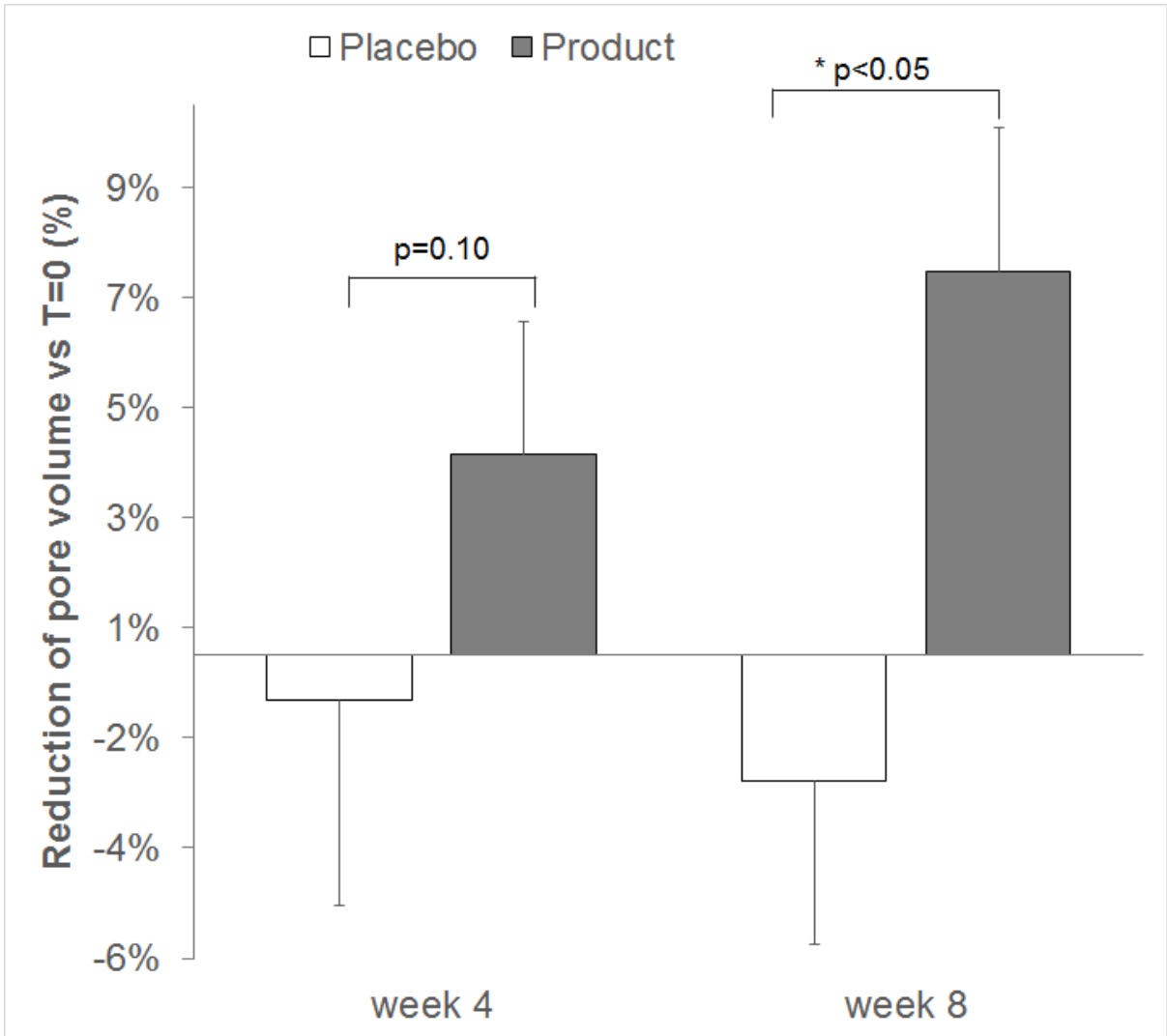


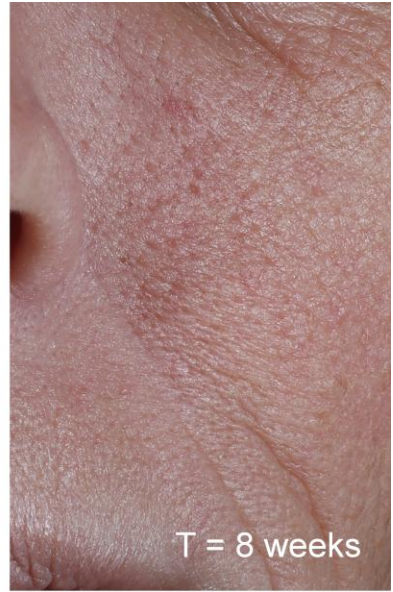


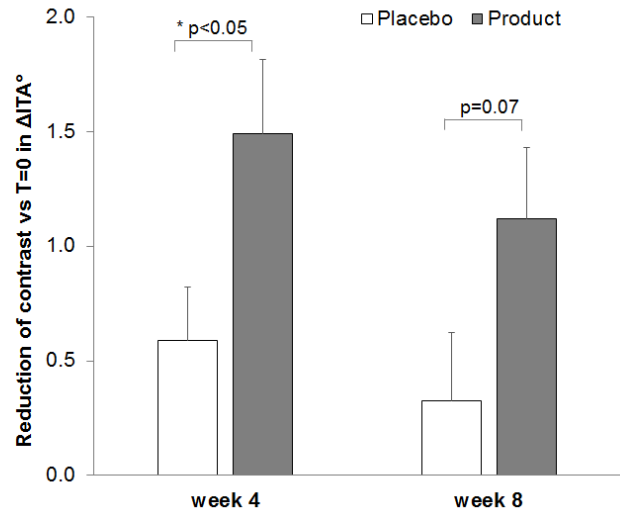
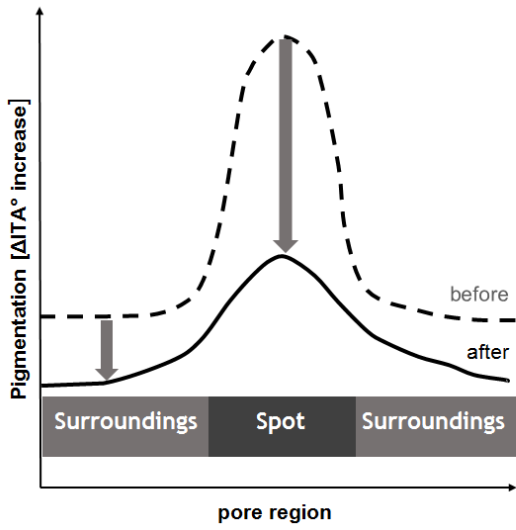
	10ng/ml TGFbeta to control		5μM 10HSA to control	
	number	in %	number	In %
Total proteins	352	100%	352	100%
% Regulated proteins, p-value <0,05	141	40.1%	151	42.9%
% Non-regulated proteins, p-value >0,05	211	59.9%	201	57.1%
% Down-regulated proteins, p-value <0,05, fold change <0,5	14	4.0%	18	5.1%
% Down-regulated proteins, p-value <0,05, fold change 0,5 to 1	65	18.5%	54	15.3%
% Up-regulated proteins, p-value <0,05, fold change 1 to 1,5	40	11.4%	39	11.1%
% Up-regulated proteins, p-value <0,05, fold change >1,5	22	6.3%	40	11.4%



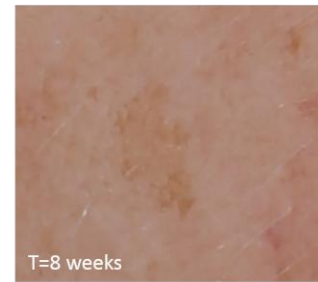
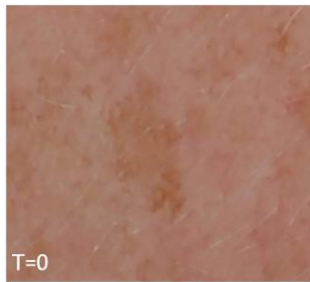








Cross-polarized images:



Projection axis using false colors:

